ELSEVIER

J. Non-Newtonian Fluid Mech., 76 (1998) 79–110

Journal of Non-Newtonian Fluid Mechanics

Relaxation of dilute polymer solutions following extensional flow[1]

Patrick S. Doyle [a], Eric S.G. Shaqfeh [a,*], Gareth H. McKinley [b], Stephen H. Spiegelberg [b]

[a] *Department of Chemical Engineering, Stanford University, Stanford, California 94305-5025, USA*
[b] *Division of Applied Sciences, Harvard University, Cambridge, MA 02138, USA*

Received 14 June 1997

Abstract

The relaxation of dilute polymer solutions following stretch in uniaxial extensional flow is investigated via Brownian dynamic simulations of a flexible freely-draining bead-rod chain. The bead-rod chain simulations are compared to Brownian dynamic simulations of a FENE dumbbell and numerical calculations of a FENE-PM chain. A universal relaxation curve for the stress decay from steady-state is found by shifting the results to lie on the curve described by the relaxation of an initially straight chain. For all the models investigated, the initial rapid decay of the polymer stress decreases at a rate which scales for large Weissenberg number, Wi as Wi^2. Our universal curve is in good qualitative and in some cases quantitative agreement with the available experimental data: it is particularly good in predicting decay after stretch at the largest strains. We find hysteresis in comparing the stress versus birefringence during the startup of flow and subsequent relaxation for the bead-rod chain and FENE dumbbell, but not for the FENE-PM chain. The hysteresis in the latter model is lost in the preaveraging of the nonlinear terms. The bead-rod model also displays a configuration hysteresis. The hysteresis observed in these models is in qualitative agreement with recent experiments involving polystyrene-based Boger fluids.

Keywords: Dilute polymer solutions; Extensional flow; Relaxation

1. Introduction

The physical mechanisms by which large stresses are generated in dilute polymer solutions subjected to extensional flows are not well understood. The development of the filament stretching rheometer has recently enabled many groups to measure the extensional stresses of dilute and semidilute polymer solutions, both during the start-up of flow and subsequent relaxation [1–3]. Upon the cessation of flow very rapid decays in the polymer stress were

* Corresponding author. Fax: +1 415 7239780.

[1] Dedicated to the memory of Professor Gianni Astarita.

0377-0257/98/$19.00
PII S0377-0257(97)00113-4

observed. The very fast nature of this decay is problematic from both an experimental and modeling point of view. First, in the experiments there is a finite time over which the velocity of the moving end-plates can be arrested and hence the flow 'stopped'. This finite time to stop the plates is on the order of 50–100 ms and the longest relaxation time for the polymers is 1–3 s. Any relaxation process which occurs on smaller time scales than 50 –100 ms cannot be unambiguously resolved. Theoretically there is not a clear understanding of whether these relaxation processes arise from viscous or elastic stresses. Furthermore, if they are elastic, how can this fast relaxation be incorporated into a constitutive equation and how is the fast relaxation process related to the polymer's longest relaxation time and/or the polymer architecture?

There have been relatively few theoretical or numerical studies of chain relaxation after elongational flow. Grassia and Hinch [4] have recently presented a comprehensive study of the stress relaxation of flexible bead-rod chains released from an initially straight configuration and Doyle, Shaqfeh and Gast [5] have also examined the stress and birefringence relaxation of initially straight chains. Both studies include the results that the initially straight chains have $O(N^3)$ stresses and a characteristic long relaxation time which scales as N^2 where N is the number of beads in the chain. Grassia and Hinch showed that the initial stress decayed exponentially on $O(\xi a^2/kT \times 1/N^2)$ time scales where ξ is the drag on a bead, a is the connecting rod length and kT the Boltzmann energy. Doyle et al. found that the birefringence initially decayed exponentially on $O(\xi a^2/kT)$ time scales corresponding to the rotation of an individual link in the chain. At intermediate times, $1/N^2 < t/(\xi a^2/kT) < N^2$, Grassia and Hinch found a power law decay of $t^{-1/2}$ for the stress. In both relaxation studies the chains were initially in a straight configuration and the initial decay of the stress and birefringence corresponded to rotation of the smallest length scale in the chain.

Using the same model, Doyle et al. [5] and Rallison [6] demonstrated that the steady-state extensional stresses were dominated by the elastic contributions for $\mathrm{Wi} < 0.06N^2$, where Wi is the Weissenberg number defined as the longest relaxation time of the chain times the extension rate (see Section 2.1 for a more detailed discussion). Doyle and Shaqfeh [7] further showed that the transient extensional stresses were mostly elastic beyond a time of $0.075\xi a^2/kT$. Only in steady flows at large stretch rates, $\mathrm{Wi} \approx 0.06N^2$, did the elastic stresses approach the value for a completely straight chain [5]. The stress at finite Hencky strains and moderate Wi is less than the straight chain value [5] and so is not expected to decay at the same rate as the initially straight chains. We expect the initial decay rate for the straight chain simulations to be an upper bound and the decay rate at long times to be a lower bound on the values we obtain for stress and birefringence relaxation for stretch at finite values of Wi and finite strain. Due to the large difference of times scales in the fast and slow relaxation processes, it is worthwhile to investigate the rates of relaxation for moderate Wi and strains to determine the relaxation rates one can feasibly obtain in an experiment.

We present an investigation of the relaxation of dilute polymer solutions following extensional flow using Brownian dynamics simulations of bead-rod chains and FENE dumbbells, as well as numerical calculations of a FENE-PM model. The models are compared to the experimental data of Spiegelberg and McKinley for monodisperse polystyrene-based Boger fluids [1,8] and the data of Orr and Sridhar for polydisperse polyisobutylene-based Boger fluids [2].

We first present results for Brownian dynamics simulations of the bead-rod chains. A universal relaxation curve for the stress decay from steady-state is found by shifting the results to lie on the curve described by the relaxation of an initially straight chain. The universal relaxation curve allows us to determine a characteristic time scale over which 50% of the stress will relax. The relaxation from finite strains is discussed and compared to the FENE dumbbell and FENE-PM chain models. Furthermore, the finite ramp-down time of the motor is incorporated into the simulations and discussed in relation to the experiments. The universal stress relaxation curve is compared to the relaxation of polystyrene(PS)-based Boger fluids [1] and polyisobutylene(PIB)-based Boger fluids [2].

The start-up and the subsequent relaxation of the stress and birefringence for polystyrene-based Boger fluids [8] is compared to the FENE-PM model, FENE dumbbell and to a FENE dumbbell model with a conformation dependent drag coefficient. Hysteresis is observed when comparing the stress versus birefringence during start-up and in the subsequent relaxation in both the experiments and in the bead-rod chain and FENE models, but not in the FENE-PM model. The physical and numerical origins of the hysteresis are discussed.

2. Polymer models

The simulation algorithms and development is presented in detail elsewhere [5,7]. We present here a brief overview of the models.

2.1. Flexible bead-rod chain

The flexible bead-rod chain model consists of a series of beads which are connected via rigid rods of length a which serve to hold the beads at a constant interbead separation [9]. The length scale a corresponds to a Kuhn step in the polymer [10]. Stochastic Brownian forces are included to model the solvent collisions acting on the beads [11,12]. The chains are freely-draining, i.e. hydrodynamic interactions have been neglected. The drag on a bead is ξ and the characteristic diffusive time scale is $\xi a^2/kT$. The flow strength is characterized by the chain Weissenberg number as the product of the longest chain relaxation time, $\lambda_1 = 0.0142N^2\xi a^2/kT$, obtained from previous simulations [5] and the extension rate $\dot{\epsilon}$, $\mathrm{Wi} = \lambda_1\dot{\epsilon}$.

The chain trajectories are calculated using a Brownian dynamics algorithm developed by Liu [13] and the polymer stress is calculated using the noise filtering technique developed by Doyle et al. [5]. Previously we have shown that the steady [5] and transient [7] stresses are dominated by the elastic components for $\mathrm{Wi} < 0.06N^2$ at times scales larger than $0.075\xi a^2/kT$ (on the order of the smallest time scale in the polymer). The viscous stress is at least an order of magnitude smaller than the elastic component [5,7] and is insignificant, thus we present only the total polymer stress in this study, while remembering that the total is, in effect, the elastic stress. A measure of the optical anisotropy of the chain is also calculated, namely the birefringence. The birefringence measures the difference in the principal eigenvalues of the index of refraction tensor [14].

In the simulation averages are taken over ensembles of 100–1000 chains. In considering the bead-rod chain, all lengths are made dimensionless with the bead diameter a, stress with $n_\mathrm{p}kT$ where n_p is the number density of polymer molecules in solution and the birefringence with

$$n_p(\alpha_1 - \alpha_2)\frac{4\pi}{3}\frac{(n^2+2)^2}{6n}$$

where n is the isotropic part of the index of refraction, α_1 is the polarizability parallel to a connecting rod in the chain and α_2 is the polarizability perpendicular to a rod. In general there are a number of different interesting time scales and these include, primarily λ_1 and $(\dot{\epsilon})^{-1}$. However the bead diffusion time $\xi a^2/kT$ is also a useful scale. Thus, we shall endeavour to write explicitly the nondimensionalization of time (using t always as a dimensional variable) in all contexts and reserve the symbol $\epsilon = \dot{\epsilon}t$ for the Hencky strain experienced by a material element at a time t.

2.2. FENE dumbbell

The FENE dumbbell consists of two beads joined by a nonlinear elastic spring [10]. The spring represents the entropic restoring force arising from holding the ends of a flexible bead-rod chain with N beads at a fixed end-to-end vector Q_i [10,15]. Implicit in the FENE force derivation is the assumption that the bead-rod chain can sample all configurations for a given end-to-end vector. The FENE spring force is [10,16]

$$F_i^{\mathrm{FENE}} = \frac{HQ_i}{\left[1 - \left(\frac{Q}{Q_0}\right)^2\right]} \tag{1}$$

where $Q = \sqrt{Q_i Q_i}$ and Q_0 is the maximum extensibility of the dumbbell. The parameters H and Q_0 are related to a bead-rod chain through the relations $H = 3kT/(N-1)a^2$ and $Q_0 = (N-1)a$. The relaxation time for the FENE dumbbell is $\lambda_H = \zeta/4H$ where ζ is the drag on one bead in the dumbbell and the dimensionless extensibility parameter is $b = HQ_0^2/kT$. For large N, the extensibility parameter b is equal to $3N$. When comparing the FENE model to the bead-rod chains or the experimental data we will chose b based on the number of Kuhn steps in the polymer.

Brownian dynamics simulations are performed using the semi-implicit predictor corrector method proposed by Ottinger [12,17] to solve for the trajectories of the dumbbells. Ensemble averages are taken over populations of 10^4 dumbbells. In considering FENE dumbbells, all lengths are made dimensionless with $\sqrt{kT/H}$, and stress with $n_p kT$. A Weissenberg number for the dumbbell is defined by $\mathrm{Wi}^{\mathrm{FENE}} = \lambda_H\dot{\epsilon}$. The FENE birefringence has been made dimensionless in the same way as for the bead-rod chain, namely with $n_p(\alpha_1 - \alpha_2)\frac{4\pi}{3}\frac{(n^2+2)^2}{6n}$.Again, we shall write out explicitly the time nondimensionalization, and in general the important time scale is λ_H.

2.3. Conformation dependent drag FENE dumbbell

The drag on a polymer will increase as it is unravelled by the flow. A conformation dependent drag coefficient is a simple means to account for the additional drag on an uncoiled chain

[18–20]. In our conformation dependent drag FENE(FENE-CD) simulations, the drag on a bead increases linearly with the end-to-end distance from a value of ζ_0 at equilibrium to ζ_{max} at full extension [7]. This introduces a new parameter ζ_{max}/ζ_0, in addition to the standard FENE parameters. To estimate ζ_{max}/ζ_0 we have calculated the ratio of the drag on a straight rod to the drag on a Zimm chain [21]

$$\frac{\zeta_{max}}{\zeta_0} = \frac{6.28L}{\ln(L/d)5.11R} \tag{2}$$

where L is the length of the chain, d is the diameter, and R is the equilibrium root-mean-square end-to-end separation of the chain. We consider this as an upper bound for ζ_{max}/ζ_0 since in the simple bead-spring dumbbell model we place all the drag on two beads at the end of the chain [22]. When comparing the FENE-CD model to experimental data we use ζ_{max}/ζ_0 as an adjustable parameter to obtain the best fit.

Brownian dynamics simulations are performed using the semi-implicit predictor corrector method proposed by Ottinger [12,17] to solve for the trajectories of the dumbbells. Ensemble averages are taken over populations of 10^4 dumbbells. The relaxation time for the FENE-CD dumbbell is $\lambda_H^{CD} = \zeta_0/4H$ and the dimensionless extensibility parameter is $b = HQ_0^2/kT$. In considering FENE-CD dumbbells, all lengths are made dimensionless with $\sqrt{kT/H}$, and stress with $n_p kT$. A Weissenberg number for the dumbbell is defined by $\mathrm{Wi}^{FENE-CD} = \lambda_H^{CD}\dot{\epsilon}$. The FENE-CD birefringence has been made dimensionless in the same way as for the bead-rod chain, namely with $n_p(\alpha_1 - \alpha_2)\frac{4\pi}{3}\frac{(n^2+2)^2}{6n}$. In general the important time scale is λ_H^{CD} and we shall write the time nondimensionalization explicitly.

2.4. FENE-PM model

The linear springs in a Rouse chain can be replaced by M FENE springs, but the viscometric properties of the resulting model cannot be solved analytically [10]. The FENE-PM model [23] replaces the squared length of each spring in the denominator of the FENE force law with the average taken over all configurations and springs in a chain. After taking the limit as the number of modes approaching infinity, the relaxation times for the modes ($\alpha = 1, 2, \ldots, M$) are related via the expression $\lambda^{R,\alpha}/\lambda^{R,1} = 1/\alpha^2$ [10,24] where $\lambda^{R,1}$ is the slowest mode and is equal to the slowest mode in a Rouse chain.

Note that in modeling a chain with a fixed number of Kuhn-steps, the number of modes and the extensibility parameter in the FENE-PM springs should not be varied independently and for large chains are related by the condition $3b \times M = N$ [12,23]. The constitutive equation for the FENE-PM chain is a system of coupled differential equations [7,23] which are solved numerically using a fourth order Runge–Kutta method [25]. In further discussion of the FENE-PM chain stress has been made dimensionless with $n_p kT$, and birefringence with $n_p(\alpha_1-\alpha_2)\frac{4\pi}{3}\frac{(n^2+2)^2}{6n}$. The Weissenberg number is based on the longest relaxation time, and when necessary, we will again show any time nondimensionalization explicitly.

3. Simulation results and important scalings

In this section we discuss the relaxation of polymer (bead-rod) chains following uniaxial extensional flow where the primary axis of extension of the flow is in the '1' direction. In Fig. 1 we show the relaxation of the polymer stress from the steady-state value in extensional and also shear flow for a range of Wi and N. In extensional flow the rate of relaxation rapidly increases as the Weissenberg number increases. The results for several values of N are shown for $\mathrm{Wi} = 10.65$ and collapse onto the same curve. The relaxation of the shear stress is much slower than the extensional stress for $\mathrm{Wi} > 1.065$. For $\mathrm{Wi} = 1.065$, the shear stress τ_{12}^{p} and extensional stress relax identically while the normal stress difference $\tau_{11}^{p} - \tau_{22}^{p}$ relaxes more slowly. This can be understood by considering the Rouse model in which each mode α relaxes exponentially with a characteristic time $\lambda^{R,\alpha}$ [10]. For a large number of modes [24], the modes are related via the expression $\lambda^{R,\alpha}/\lambda^{R,1} \approx 1/\alpha^2$ where $\lambda^{R,1}$ is the slowest mode. At steady-state in shear flow, $\tau_{12}^{p} \propto \Sigma\, \lambda^{R,\alpha}$ and $\tau_{11}^{p} - \tau_{22}^{p} \propto \Sigma(\lambda^{R,\alpha})^2$. Thus due to the spacing of the modes, τ_{12}^{p} has a larger contribution from the faster modes and hence decays faster than $\tau_{11}^{p} - \tau_{22}^{p}$. The simulation

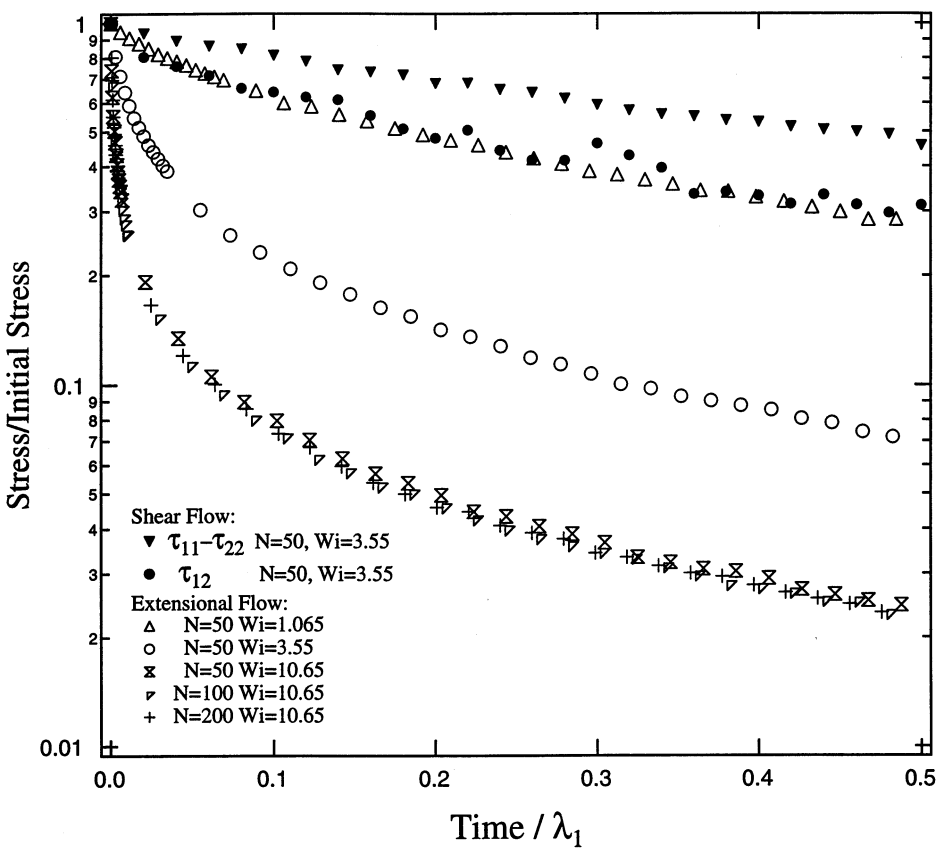

Fig. 1. Relaxation of the the bead-rod chain polymer stress from the steady-state value in extensional and shear flow versus time divided by the longest relaxation time. For extensional flow the polymer stress difference, $\tau_{11}^{p} - \tau_{22}^{p}$, is shown and for shear flow both $\tau_{11}^{p} - \tau_{22}^{p}$ and τ_{12}^{p}. The stress is divided by the value when flow is stopped.

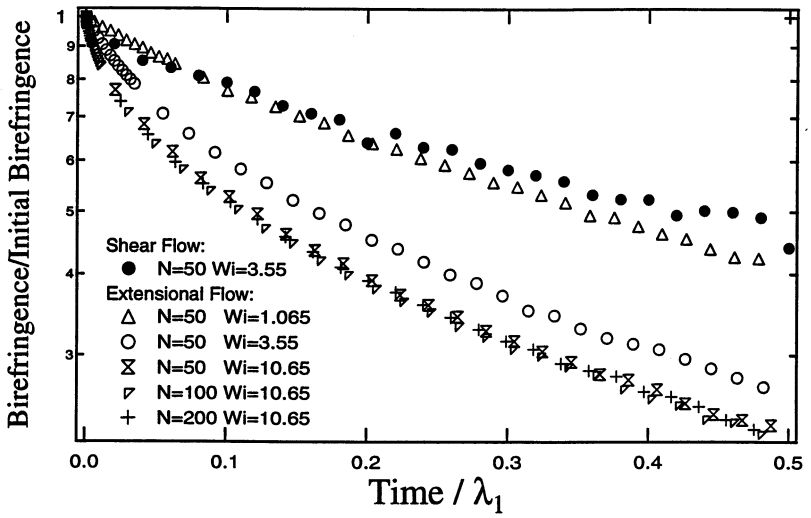

Fig. 2. Relaxation of the bead-rod chain polymer birefringence from the steady-state value in extensional and shear flow versus time divided by the longest relaxation time. The birefringence is divided by the value when flow is stopped.

results in Fig. 1 are qualitatively very similar to those of Fig. 4 in Spiegelberg and McKinley [1] for the relaxation of polystyrene-based Boger fluids. We will return to a quantitative comparison in due course.

In Fig. 2 we show the birefringence relaxation from the steady state value for the same range of N and Wi as in Fig. 1. In a similar fashion to the stress, the birefringence relaxes faster as Wi increases and for $\mathrm{Wi} = 1.065$ the birefringence arising in shear and extensional flow relax almost identically. Also, for $\mathrm{Wi} = 10.65$ the curves coincide for various values of N. However, the birefringence relaxes much more slowly than the stress for $\mathrm{Wi} > 1.065$.

In extensional flow, the flexible bead-rod chains are extended almost completely straight at steady-state for $\mathrm{Wi} \geq 1$. One might speculate then that the relaxation of the stress and birefringence should be similar to the relaxation of an initially completely straight chain aligned along the primary axis of extension, the '1' direction. In Fig. 3(a) we show the stress relaxation from steady state in extensional flow compared to the relaxation of an initially straight chain with $N = 100$. Note the initial value of the stress for a straight chain with $N = 100$ is 333399 and scales as N^3 [4,5]. (This stress must be completely Brownian stress since there is no flow ever applied to the straight chain in this calculation.) In Fig. 3(a) we only show the portion of the straight chain relaxation curve in which the scaled stress is of comparable magnitude to the extensional flow stresses. For the relaxation from extensional flow the time has been shifted by an additive term such that the initial stress lies on the relaxation curve for the initially straight chain. The value of this dimensionless shift factor is different for each value of Wi, but does not significantly change with increasing N at a fixed $\mathrm{Wi} = 10.65$. This can be understood by considering the asymptotic expression for the steady-state viscosity at large Wi [5,26]:

$$\eta^{\mathrm{p,ss}} = (1 - 0.34/\mathrm{Wi})N(N^2 - 1)/12 \tag{3}$$

where the viscosity has been made dimensionless with $n_p\xi a^2$. (Note that this expression is derived for the total stress of the bead rod chain including the viscous stresses [5,26]. However, as we have shown elsewhere and discussed above the Brownian stresses dominate for $\mathrm{Wi} < 0.06N^2$. Thus this result is a very good approximation for the Brownian stresses for almost all reasonable values of Wi, and therefore can be used to understand the relaxation of Brownian stresses.) By combining Eq. (3) with the expression $\lambda_1 = 0.0142N^2\xi a^2/kT$ and assuming N is large, the scaled extensional stress difference at large Wi can then be rewritten as

$$\frac{\tau_{11}^p - \tau_{22}^p}{N-1} = 5.87\mathrm{Wi} - 2 \tag{4}$$

where we recall that $\tau_{11}^p - \tau_{22}^p$ has been made dimensionless with n_pkT. Thus the steady-state extensional stress divided by $N-1$ is only a function of Wi and the magnitude of the time shift in Fig. 3 should also depend only on Wi. It is remarkable that by merely shifting the time all the stress curves collapse onto a universal curve described by the relaxation of an initially

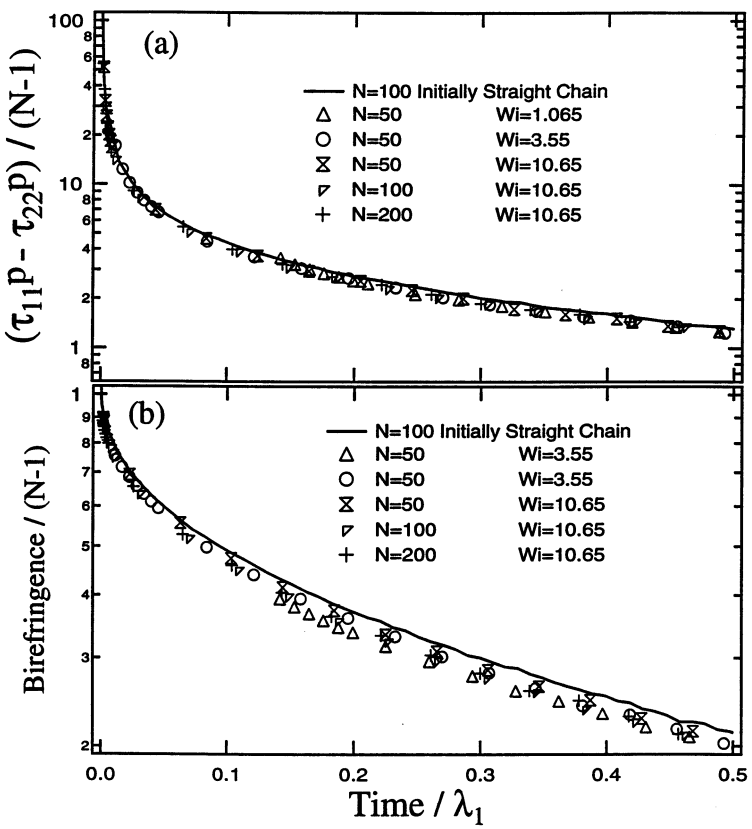

Fig. 3. (a) Relaxation of the bead-rod chain polymer stress from the steady-state value in extensional flow versus time. The solid line denotes the relaxation of an initially straight chain with $N = 100$. The time for the extensional stress relaxation curves has been shifted so that the initial stress lies on the initially straight chain curve. In (b) the relaxation of the birefringence is plotted versus time. The time for the extensional birefringence relaxation curves has been shifted by the same magnitude as in (a) for the corresponding Wi.

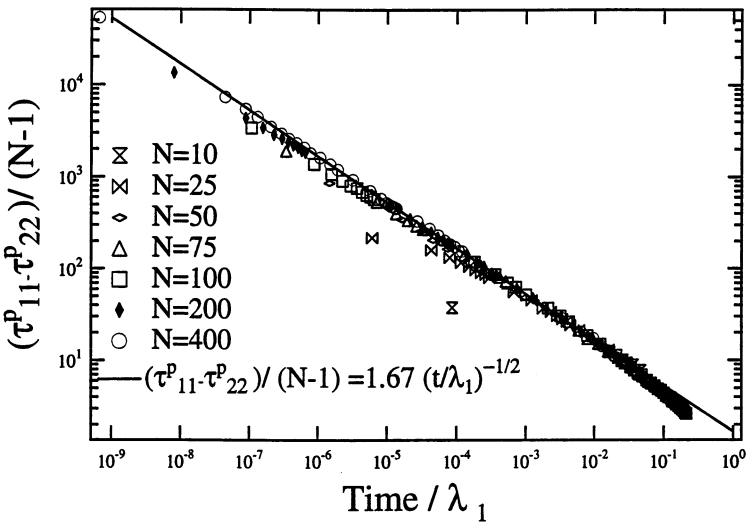

Fig. 4. Log–log plot of the stress versus time for the relaxation of initially straight bead-rod chains. The symbols denote relaxation for $N = 25$–400 and the line is a fit to the power law region which decays as $t^{-1/2}$.

straight chain. In Fig. 3(b) we show the relaxation of birefringence for the same range of N and Wi as in Fig. 3(a). The time for the relaxation curves following flow have been shifted by the same amount as in Fig. 3(a) and these curves also collapse very near to the curve for the relaxation of an initially straight chain. However, unlike the stress, the birefringence at $t = 0$ is close to the maximum value for a straight chain, $N - 1$. Note that a similar universal curve describing stress relaxation for the FENE-P (i.e. FENE-PM with $M = 1$) dumbbell model is described in Appendix A.

Having shown that the stress and birefringence can be collapsed onto the curves described by the relaxation for initially straight chains we turn now to a discussion of the important scalings for relaxation of an initially straight chain. Hinch and Grassia [4] have done an extensive study of the stress relaxation for initially straight chains and Doyle et al. [5] have examined the birefringence and stress relaxation under the same conditions. The straight chains have a finite stress [4,5] equal to $(N^3/3 + 2N/3 - 1)$ which decays on $O(\lambda_1/N^4)$ time scales [4]. At long times, the stress is $O(N - 1)$ and decays exponentially over λ_1, time scales [5,4]. At intermediate times the stress is $O(N^2)$ and decays as $t^{-1/2}$ [4]. We now must consider what portion of the stress relaxation curve for initially straight chains is relevant to the relaxation from extensional flow. Our simulations and Eq. (4) demonstrate that the steady-state extensional stress will be $O(N\mathrm{Wi})$, however in Fig. 3 the initial stress decay is not a simple exponential. Thus we must consider the power-law behavior described by Grassia and Hinch [4] at intermediate times and the transition to exponential decay at long times. Grassia and Hinch worked with relatively small chains, $N \leq 10$, in their study of the intermediate-to-long time scalings. We have performed additional simulations with much longer chains, $N \leq 400$, to better assess over what region the power-law behavior will hold and how this will change with increasing N. In Fig. 4 we show the stress divided by $N - 1$ versus time divided by λ_1 for chains which are initially aligned straight in the '1' direction. Plotted in a log-log manner the data clearly shows the power-law decay described

by Grassia and Hinch [4]. The best fit to the data in the power-law region is given by the solid line, $(\tau_{11}^{p} - \tau_{22}^{p})/(N-1) = 1.67(t/\lambda_1)^{-1/2}$ which is very close to the value reported by Grassia and Hinch [4], $1.49(t/\lambda_1)^{-1/2}$. The time where the stress first begins to obey the power-law decay decreases as N increases. For $N = 400$ the stress begins to show power-law decay when it is $O(10^4)$ (i.e. $t/\lambda_1 \approx O(10^{-7})$) which would correspond to a steady-state extensional stress at $Wi \approx 1700$. At much longer time scales, deviations from the power-law behavior occur when $t/\lambda_1 \approx 0.1$ or $(\tau_{11}^{p} - \tau_{22}^{p})/(N-1) \approx 8-10$, but the data for all N still fall on the same universal curve. Thus the magnitude of the relaxing polymer stress following cessation of homogeneous extensional flow for all reasonable Wi will fall on the stress relaxation curve in Fig. 4 in a region in which the data collapses onto a universal curve when scaling the dimensional stress with $n_p kT(N-1)$ and time with λ_1. Furthermore, the starting point for the relaxation after extensional flow can be determined using Eq. (4) and thereafter the stress will relax along the master curve. Again, we refer to Appendix A for the equivalent master curve for relaxation of stress in the FENE-P dumbbell model.

In a similar manner, the birefringence relaxation for initially straight chains can be described by a master curve. In Fig. 5 the birefringence divided by $N-1$ is plotted versus time divided by λ_1. As N increases, the curves begin to collapse onto a single curve. The inset of Fig. 5 shows the birefringence at small times which also converge as N increases. Previously Doyle et al. [5] showed that the dimensionless birefringence initially decays as $\Delta' = (N-1)(1 - 12kTt/a^2\xi)$ for $kTt/a^2\xi \ll 1/12$ and decays exponentially at long times as $\Delta' = (N-1)e^{-t/\lambda_1}$. Another way to express this result is that the birefringence will decay as $\Delta' = (N-1)(1 - 0.17N^2 t/\lambda_1)$ for $t/\lambda_1 \ll 5.87/N^2$. In the limit of large N, there will thus appear to be a birefringence 'jump' when plotting Δ' versus t/λ_1, but the magnitude of this apparent jump will be very small as seen in the inset of Fig. 5. Note that this occurs because the birefringence is $O(N)$ for both the short time and long time scalings. While the initial relaxation of the birefringence in Fig. 5 cannot be

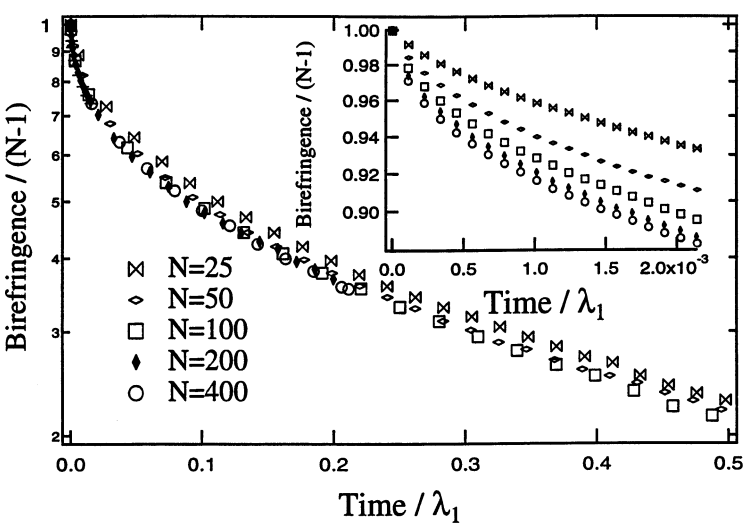

Fig. 5. Semilog plot of the birefringence versus time for initially straight chains with $N = 25$–400. The inset plot shows the birefringence at short times.

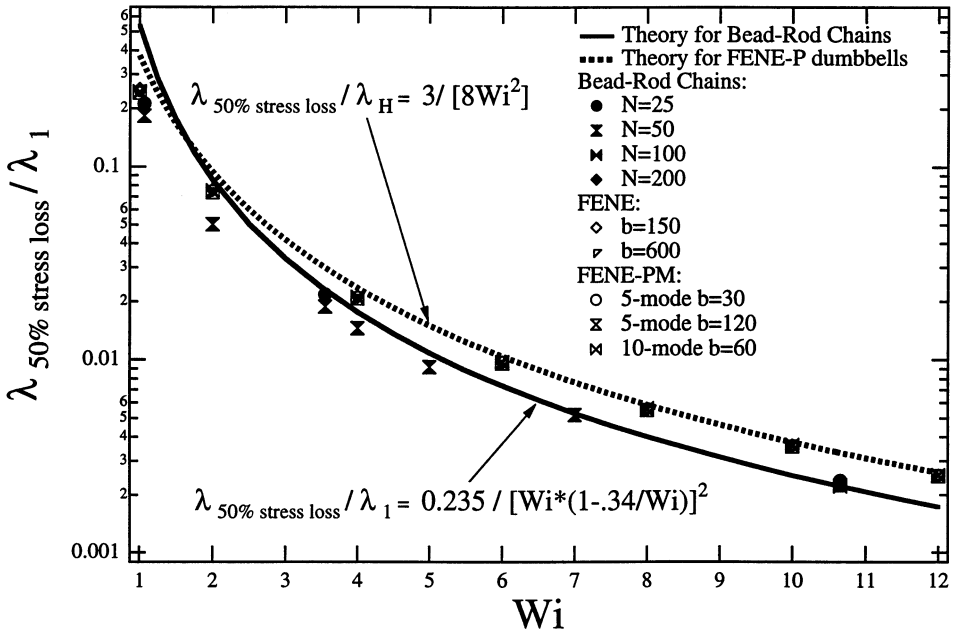

Fig. 6. Characteristic time, $\lambda_{50\%\ \text{stress loss}}/\lambda_1$, for the polymer stress to reach 50% of initial value at steady state versus Wi. Symbols denote results for bead-rod chains, FENE dumbbells and FENE-PM model. The solid line denotes the theory presented in the text which is valid for large Wi for the bead-rod chains, and the dashed line is the theory developed in the Appendix which is valid for FENE-P dumbbells.

described by a single exponential, the initial fast relaxation is not nearly as rapid as found for the stress.

To quantify the relaxation rate of the steady-state extensional stress we have defined a characteristic time over which the stress decreases to 50% of the initial value when the flow stopped. In Fig. 6 we plot the characteristic time versus Wi. The symbols denote simulation results for bead-rod chains, FENE dumbbells and the FENE-PM model. The solid line given by

$$\frac{\lambda_{50\%\text{stress loss}}}{\lambda_1} = \frac{0.24}{(\text{Wi} - 0.34)^2}, \tag{5}$$

was obtained by assuming the stress decays as $(\tau_{11}^{\text{p}} - \tau_{22}^{\text{p}})/(N-1) = 1.67(t/\lambda_1)^{-1/2}$ and that the initial value of the stress is given by Eq. (4). Eq. (5) is in good agreement with the bead-rod chain simulations for large Wi (Fig. 6). In Fig. 6, we show that the characteristic decay times for the FENE and FENE-PM models at $\text{Wi} > 2$ are indistinguishable for various values of b and various numbers of modes. Previously Doyle and Shaqfeh [7] showed that the FENE-PM stress in steady extensional flow is dominated by the contribution from the slowest mode and hence the relaxation should proceed as if it was a single-mode FENE-P model with an effective FENE parameter $b_{\text{eff}} = b \times M$, where we recall that M is the number of modes in the FENE-PM model. Thus we need to examine why the FENE and FENE-P models relax similarly at a given Wi for all b.

First we consider the FENE dumbbell. At large $\mathrm{Wi}^{\mathrm{FENE}}$ the dumbbells are aligned almost completely in the '1' direction and the magnitude of τ_{11}^{p} is much larger than τ_{22}^{p}. Assuming τ_{22}^{p} is negligible, then $\tau_{11}^{p} \approx 2b\mathrm{Wi}^{\mathrm{FENE}}$ [10]. Furthermore, since the distribution of the dumbbell lengths is very narrow [27] we can approximate the distribution by a δ function. Neglecting Brownian motion, which is initially much smaller than the elastic restoring force, and assuming the only nonzero component of Q_i is Q_1, the rate of change of the stress divided by the initial value is given by

$$\frac{\mathrm{d}\tau_{11}/\mathrm{d}(t/\lambda_H)}{2b\mathrm{Wi}} = \frac{-1}{1-Q_1^2/b} - \frac{Q_1^2/b}{(1-Q_1^2/b)^2} \tag{6}$$

Since the distribution of dumbbell lengths is assumed to be a δ function, we can use the stress to determine that $Q^2 = 2b\mathrm{Wi}^{\mathrm{FENE}}/(1+2\mathrm{Wi}^{\mathrm{FENE}})$, and Eq. (6) can be rearranged to give

$$\frac{\mathrm{d}\tau_{11}/\mathrm{d}(t/\lambda_H)}{2b\mathrm{Wi}^{\mathrm{FENE}}} = -(1+2\mathrm{Wi}^{\mathrm{FENE}})^2 \tag{7}$$

Thus the rate of the initial stress decay will be independent of b. We have performed many simulations to verify Eq. (7) but do not report them here. Although the steady-state distribution of dumbbell lengths for the FENE-P dumbbell is very broad [27], the previous development is still valid. This follows from the fact that FENE-P model preaverages the stress and the FENE force, thus setting the nonlinear term in the denominator of the FENE force equal to the ensemble average. It follows that the model is completely described by the second moment. The only difference is that the steady-state extensional stress for the FENE-P model at large $\mathrm{Wi}^{\mathrm{FENE\text{-}P}}$ is $\tau_{11} \approx (2b-2)\mathrm{Wi}^{\mathrm{FENE-P}}$ [17] instead of $2b\mathrm{Wi}^{\mathrm{FENE}}$ as in the FENE model. This difference is negligible since usually $b \gg 2$. At large Wi, all the models (FENE, FENE-PM and bead-rod) will have initial stress decay rates that scale as Wi^2 and thus increase rapidly with increasing Wi. A more detailed analysis of the stress relaxation of the FENE-P dumbbell in Appendix A shows that an analytic result can be obtained for the universal stress relaxation curve in this instance. Furthermore, this analysis yields

$$\frac{\lambda_{50\%}}{\lambda_H} \approx \frac{3}{8\mathrm{Wi}^2} \tag{8}$$

as an asymptotic result in the limit $\mathrm{Wi} \to \infty$. This result is presented in Fig. 6 by the dashed curve and it agrees very well with the full numerical results for the FENE-P.

What is striking about the relaxation times in Fig. 6 is that they are much smaller than the longest relaxation time; for example at $\mathrm{Wi} = 10$, 50% of the stress decays over a time which is merely $0.003\lambda_1$. In Fig. 7 we show sample chain configurations for $N = 200$ during relaxation from a steady-state configuration in extensional flow at $\mathrm{Wi} = 10.65$. The percentage of the original stress following the cessation of flow is shown and the time elapsed since the flow is stopped. It is clear from Fig. 7 that very small changes in the chain conformation can result in very large changes in the stress. One can visually discern that the birefringence barely changes (less than 5% change) over the time scale in which 70% of the stress has decayed. Further relaxation of the configuration proceeds from the ends inward because the outer links of the chain are under less tension than the inner ones. Perkins et al. [28] have used fluorescence microscopy to observe single DNA molecules relaxing from a stretched configuration and report

seeing the ends of the molecule formed a compact ball (with diameter of approximately 10 Kuhn steps) as it relaxed. Furthermore, Brochard-Wyart and Buguin [29] have introduced the 'Stem–Flower' model for the conformation of a polymer chain held fixed at one end and subject to a strong uniform flow. The chain relaxes to the equilibrium coil by progressive destruction of the internal 'stem' from the free end inward. The development of a ball or flower is indeed observed as we follow the relaxation of the chains (Fig. 7). We see that even at $t = 0.56\lambda_1$, the chain is still significantly stretched and aligned. The memory of the original stress has almost vanished while the memory of the alignment has not. If the flow were to be started again at $t = 0.56\lambda_1$, the response of the chain would be very different than if it were a random coil. Moreover, a stretched chain in a Lagrangian time-varying flow may not relax to its equilibrium configuration before it encounters a new region of the flow field. The response of the chain will depend on its orientation and stretch which are determined by its flow history.

In all experiments that measure polymer stress relaxation there is a finite time over which the movement of the apparatus creating the flow can be arrested and hence the 'flow stopped' [2,30]. In the filament stretching rheometer, the fastest deceleration time reported in the literature by Orr and Sridhar [2] is 50 ms and the flow is linearly decelerated. The longest relaxation time for the commonly used Boger fluids is $\lambda_1 = 1 - 4$ s [1,2]. Thus the deceleration time is $0.0125 - 0.05\lambda_1$ and is thus comparable to the simulated characteristic relaxation times in Fig. 6. To better assess the affects of a finite deceleration time we have performed additional relaxation simulations in which the Weissenberg number is linearly decreased from the original flow value to zero. In Fig. 8 the stress relaxation from the steady-state value at $\mathrm{Wi} = 3.55$ for $N = 50$ is plotted versus time. In the simulations the flow has been linearly ramped from $\mathrm{Wi} = 3.55$ to $\mathrm{Wi} = 0$ over the times indicated in Fig. 6. The characteristic time for a 50% stress decay at $\mathrm{Wi} = 3.55$ with a zero deceleration time (i.e. instantaneous cessation of extension) is $0.016\lambda_1$. Clearly, the finite deceleration of the flow can significantly affect the stress relaxation. Over the time scale during which the flow is decelerated, the stress decays almost linearly, as can be seen most easily for deceleration times of $0.03\lambda_1$ and $0.1\lambda_1$. The steady-state extensional stress has been shown earlier to be linear in Wi, Eq. (4). The dimensionless stretch rate decreases linearly

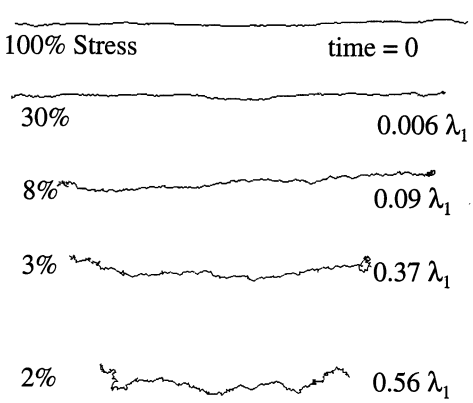

Fig. 7. Sample chain configurations during relaxation for $N = 200$ relaxing from a sample steady-state configuration at $\mathrm{Wi} = 10.65$. The percentage of the polymer stress, defined as the polymer stress divided by the stress when the flow was stopped at time = 0, remaining after the flow ceases is also shown.

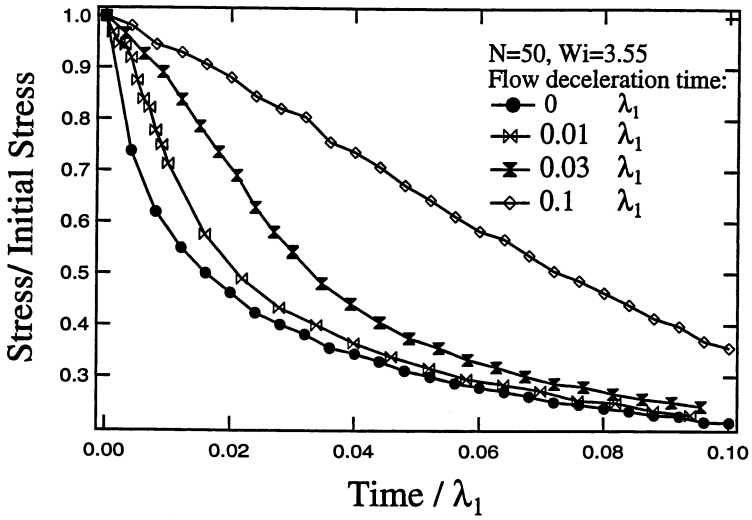

Fig. 8. Polymer stress, $\tau_{11}^{p} - \tau_{22}^{p}$, divided by steady-state stress versus time for relaxation from steady-state at $N = 50$, $\mathrm{Wi} = 3.55$. The flow is linearly ramped down starting at time $\lambda_1 = 0$ from $\mathrm{Wi} = 3.55$ to $\mathrm{Wi} = 0$ over a time of $0 - 0.1\lambda_1$.

as the flow is decelerated, and the stress is quasi-steady in that it can respond to the flow much faster than the flow is changing. In other words if λ_{decel} is a characteristic time for the motor to decelerate (e.g. the reciprocal of the deceleration rate) then if the 50% stress relaxation time, $\lambda_{50\%}$, is such that $\lambda_{50\%}/\lambda_{\mathrm{decel}} < 1$ the chain responds in an almost instantaneous or 'quasi-steady' fashion to the motor deceleration. Eventually the Weissenberg number of the flow becomes small and the corresponding steady-state stress at that current Wi decreases faster than the chain can respond.

Orr and Sridhar [2] have denoted the stress that decays rapidly during the deceleration of the flow as 'viscous dissipation' and they have further defined it as equal to the difference in the stress at the time when the deceleration of the flow begins and the stress as the end of the deceleration time. They recognize that the experiment can not distinguish between an instantaneous stress decay and a fast elastic stress decay of duration less than 50 ms. The viscous dissipation (defined in this way) is found to scale as Wi [2]. In Fig. 9 we show results for simulations in which the velocity is decelerated over a time of $0.06\lambda_1$. The stress is separated into the stress remaining when the $\mathrm{Wi} = 0$ at $t = 0.06\lambda_1$, i.e. the apparent elastic stress, and the difference in the stress at $\mathrm{t} = 0$ and at $\mathrm{t} = 0.06\lambda_1$, i.e. the apparent viscous stress. Assuming that the stress is quasi-steady, the rate of change of the stress is equal to the rate of deceleration, $\mathrm{Wi}/0.06\lambda_1$. The apparent viscous stress should then scale linearly in Wi which is consistent with the results in Fig. 9 and the experiments of Orr and Sridhar [2].

It is very difficult to experimentally measure steady-state extensional stresses. Furthermore, most other flows of interest, such as flow past a sphere [31] or through a contraction [32], are Lagrangian unsteady and there is only a finite extensional strain that a polymer will experience. It is thus important to consider the response of the stress at finite strains. In Fig. 10(a,b) we show the start-up and relaxation of the polymer stress for $N = 100$ at $\mathrm{Wi} = 10.65$ and

comparison to the FENE, FENE-PM and Rouse models. The flow is stopped after a total strain of 1, 2, 3, 6. The rate of the stress decay is a strong function of total strain for all the models. For strains $\epsilon \approx 1-2$, the FENE-PM model is in very good agreement with the bead-rod chain while the FENE model is in poor agreement. At strains $\epsilon \approx 3$ and $\epsilon \geq 6$ the FENE model is in excellent agreement with the bead-rod chain both qualitatively and quantitatively. The FENE-PM model is in good agreement with the bead-rod chain for strains of 1–2 while at a strain of 3 it relaxes much more slowly than the FENE or bead-rod model. However, at a strain of 6 the relaxation of the FENE-PM stress is very similar to both the FENE and the bead-chain results. In Fig. 10(b) the bead-rod chain is compared to a Rouse chain with 10 modes. The Rouse chain is in very good agreement with the bead-rod chain for a strain of 1 and the agreement becomes progressively poorer for larger strains. The FENE-PM model in Fig. 10(a) and the Rouse chain results are identical at a strain of 1. Note that the rate of stress decay of the Rouse chain decreases with increasing strain.

In Fig. 11(a,b) we plot the characteristic time for 50% of the bead-rod chain initial stress to decay versus total Hencky strain before the flow stops. In Fig. 11(a) for $N = 50$ the relaxation time monotonically decreases with increasing strain for all Wi. Also shown in Fig. 11(a) are the results for $N = 100$, 200 at $\mathrm{Wi} = 10.65$. At large strains the relaxation times are nearly identical which agrees with the universal relaxation description from steady-state discussed earlier. What is interesting is that at a strain of 2 the relaxation time increases with increasing N and this relaxation time is larger than the value at a strain of 1. We can better understand this by considering the relaxation times in Fig. 11(b) for $\mathrm{Wi} = 10.65$. First, the FENE model (or the FENE-P dumbbell) predicts a relaxation time which will always decrease with increasing total strain. As the dumbbells experience a larger strain the restoring force becomes increasingly

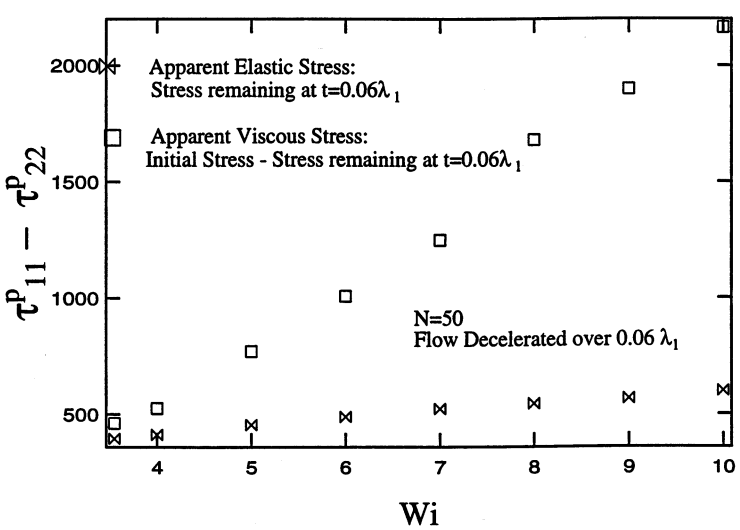

Fig. 9. Polymer stress, $\tau_{11}^{p} - \tau_{22}^{p}$ versus Wi for relaxation from steady-state of chains with $N = 50$. The flow has been decelerated over a time of $0.06\lambda_1$. The stress is separated into an apparent viscous stress equal to the difference in the initial stress when the flow stops at $t = 0$ and the stress at $t = 0.06\lambda_1$. The apparent elastic stress is the stress remaining at $t = 0.016$.

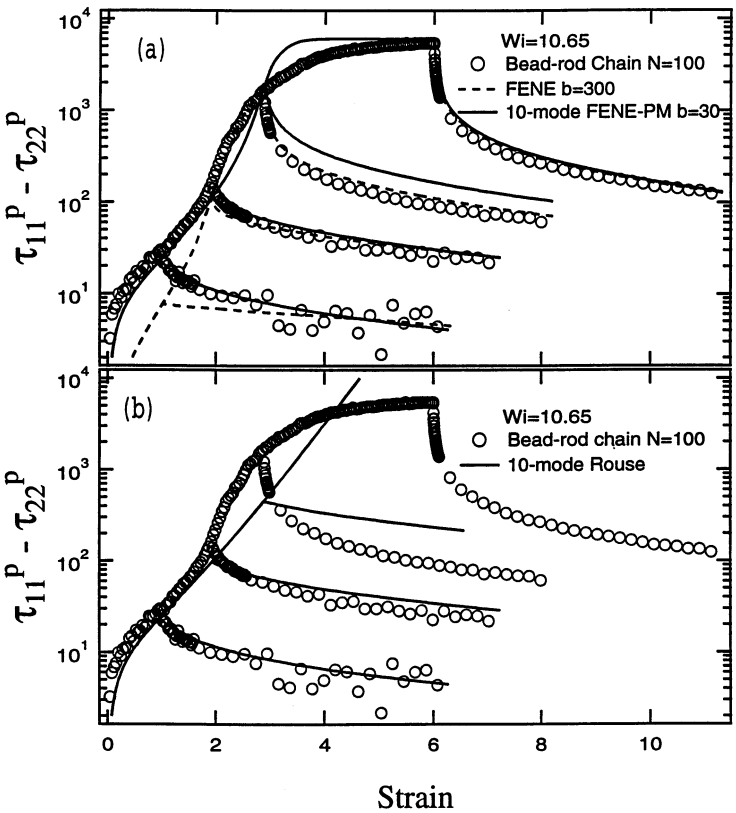

Fig. 10. Start-up and relaxation of polymer stress for $N = 100$ and $\mathrm{Wi} = 10.65$ versus strain. The strain during relaxation is defined based on the strain-rate during flow, strain = Wi × time. In (a) the bead-rod chain model is compared to a FENE dumbbell with $b = 300$ and a 10-mode FENE-PM model with $b = 30$. In (b) the bead-rod chain is compared to a 10-mode Rouse chain. The stress relaxation is shown from total strains of 1, 2, 3, 6.

nonlinear and the stress decays faster. Conversely, the Rouse model predicts that the relaxation time will always increase with increasing strain. In the Rouse model the springs have a linear response and the fast relaxation times are due to contributions from fast modes. The relaxation time for each mode does not change with increasing strain, but the relative contribution to the stress from each mode does change. At very small strains, $\epsilon \ll 1$, all the modes contribute significantly to the stress with a dimensional linear viscoelastic contribution of $\tau_{11}^{\mathrm{p}} \approx n_{\mathrm{p}} kT\lambda^{R,\alpha}$. Thus the effective relaxation time of the stress can be quite small. At large strains, most of the fast modes saturate at a steady stress while the contribution from the longest mode continues to increase exponentially. The relaxation times for the modes in the FENE-PM model in Fig. 11(b) are equal to the Rouse chain times at small strains when the nonlinear terms are small and equal to the FENE relaxation times when the stress is dominated by contributions from the longest mode. At intermediate strains there is a local maximum in the relaxation time, precisely where the FENE and Rouse curves cross. The FENE-PM model qualitatively describes the trend in the relaxation times for the bead-rod chain with $N = 200$ at all strains and is almost quantitative at high strains. Thus multimodes are needed at small strains to correctly predict linear viscoelastic response of a polymer chain and a single nonlinear mode is sufficient at large strains.

We now turn to a comparison of the birefringence. In Fig. 12(a,b) the start-up and relaxation of the birefringence are shown for the bead-rod model with $N = 100$ at $\mathrm{Wi} = 10.65$ and compared to the predictions of elastic bead-spring models. In Fig. 12(a) the FENE-PM model is in excellent agreement with the bead-rod chain for the start-up and relaxation at strains $\epsilon \leq 2$. At a strain $\epsilon = 3$ the transient growth of the birefringence is in agreement with the bead-rod chain but the relaxation as predicted by the FENE-PM is slower than that given by the bead rod chain. For larger strains the FENE-PM model underestimates the bead-rod chain birefringence and it also relaxes more slowly. The FENE model underestimates the birefringence during start-up and shows a slower relaxation. At a strain of $\epsilon = 6$ the FENE and FENE-PM models have the same birefringence which is near to the maximum possible value of 60 for the given model parameters. The elastic dumbbell models underestimate the birefringence at large strains because the birefringence is based on the small distortion of a Gaussian coil [24]. The birefringence for a straight bead-rod chain will be larger than that of a completely straight dumbbell by factor of a 5/3. We could rescale the FENE and FENE-PM birefringence by this factor of 5/3 but this would give a poor agreement for the FENE-PM chain at moderate strains. Rescaling the FENE dumbbell predictions would improve the fit to the bead-rod chain during

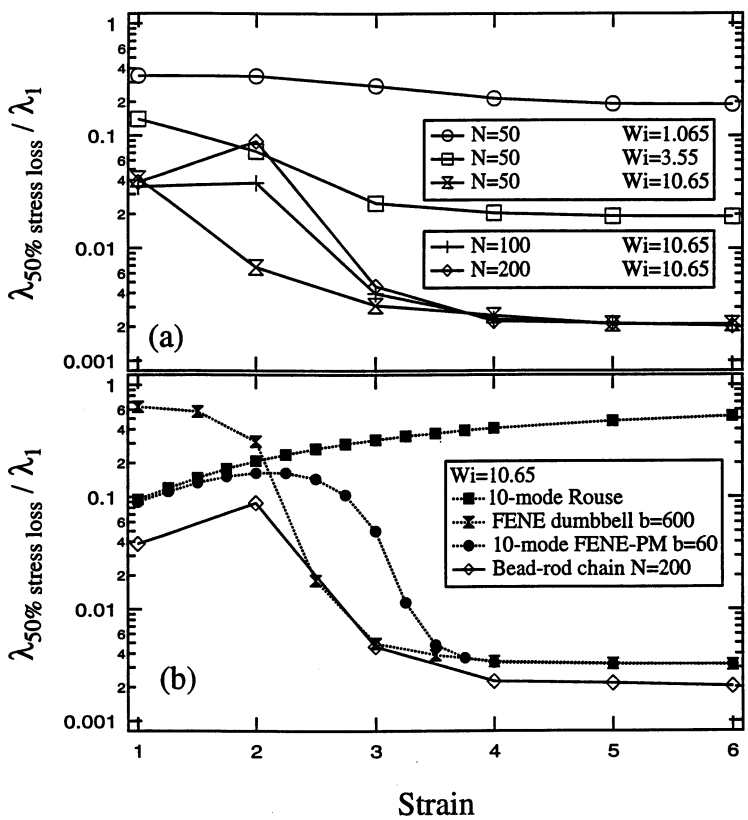

Fig. 11. Characteristic time, $\lambda_{50\%\text{stress loss}}/\lambda_1$, for the polymer stress to reach 50% of initial value at steady state versus total strain before flow is stopped.

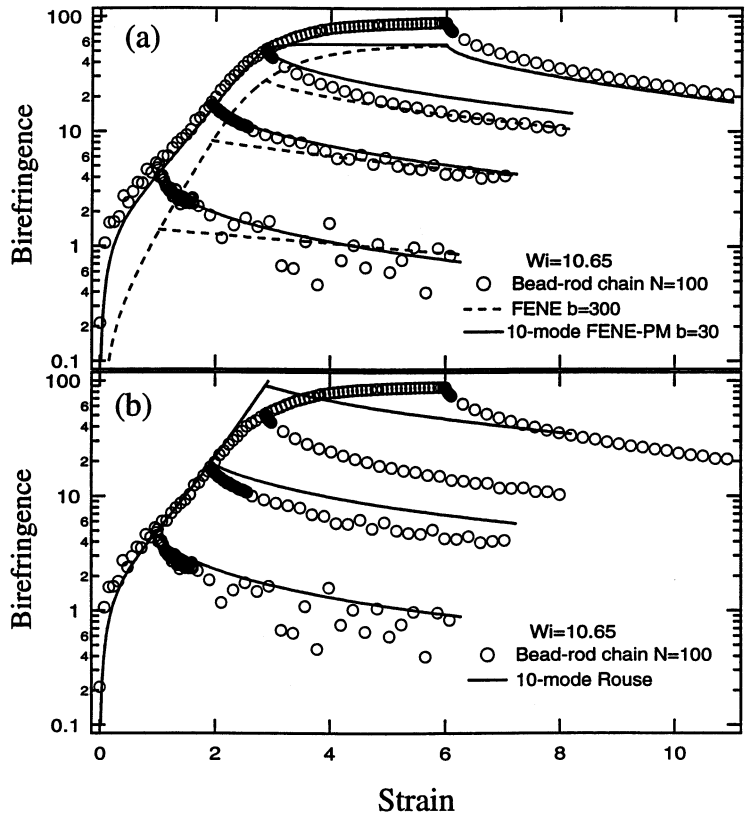

Fig. 12. Start-up and relaxation of birefringence for $N = 100$ and $\mathrm{Wi} = 10.65$ versus strain. The strain during relaxation is defined based on the strain-rate during flow, strain = Wi × time. In (a) the bead-rod chain model is compared to a FENE dumbbell with $b = 3000$ and a 10-mode FENE-PM model with $b = 30$. In (b) the bead-rod chain is compared to a 10-mode Rouse chain. The stress relaxation is shown from total strains of 1, 2, 3, 6.

start-up but not during relaxation. As we observed for the tensile stress, the FENE-PM model is in better agreement with the bead-rod chain than the FENE model during relaxation after small strains because of the presence of multiple modes in the FENE-PM model. Thus the linear Rouse model also is in good agreement with our bead rod calculations for small strains, cf. Fig. 12(b).

4. Stress-birefringence hysteresis

Another way to examine the evolution of stress and birefringence contributions from a polymer chain during the start-up and relaxation (or for that matter during any Lagrangian unsteady flow) is to plot stress versus birefringence. In a dumbbell model the birefringence is directly related to the end-to-end separation of the chain. Plotting the data in this way gives insight into the average polymer stress at a given average deformation. In Fig. 13(a) we have plotted the scaled stress difference versus birefringence for the FENE dumbbell model at several

values of the Wi and b and also for a 5-mode FENE-PM model. The simulation is run to a large strain ($\epsilon \approx 6$) such that the stress and birefringence attain their steady-state values. For a given Wi, the FENE results for chain extensibilities $b = 150$ and 600 collapse onto a single curve. We have performed simulations for many values of b and Wi which also show the same collapse but only representative results for a few values of b and Wi are shown in Fig. 13(a) for clarity. For the FENE dumbbell, during transient elongation the stress proceeds along the upper branch of the loop and reaches a maximum corresponding to the steady-state value. Then when the flow is stopped, the stress rapidly relaxes along the lower branch of the loop. There is thus a pronounced hysteresis in following the stress versus birefringence during start-up of extensional flow and relaxation after flow is stopped. As the Wi increases, the degree of hysteresis for the FENE dumbbell in Fig. 13 (a) increases. By contrast, the FENE-PM model however does not show any hysteresis because of the preaveraging. In fact, there can be no such stress/conformation or stress/birefringence hysteresis in a FENE-P or FENE-PM chain, or, in fact, in any model in which the polymeric stress is written as a function of just the second moment of the

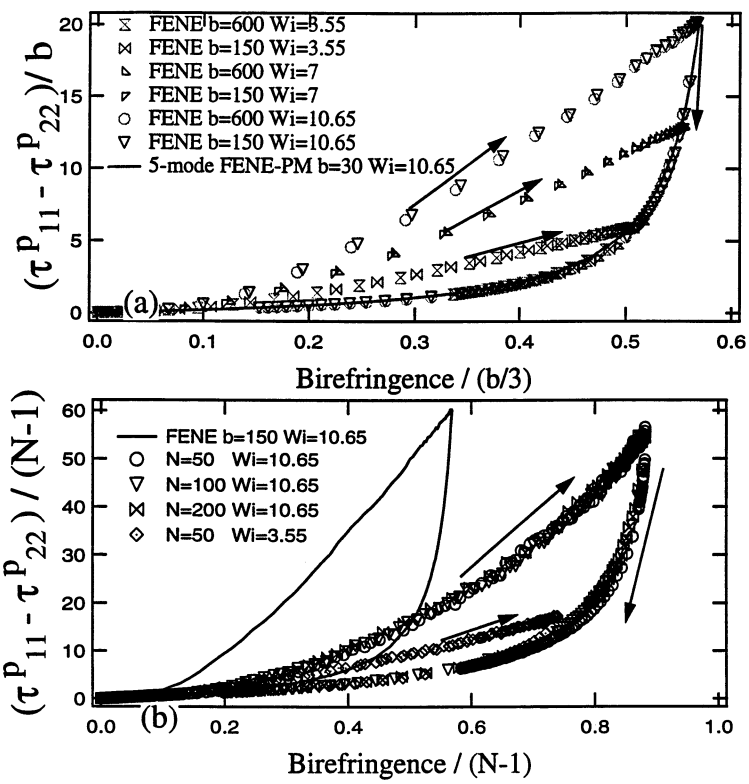

Fig. 13. Polymer stress versus birefringence for start-up of extensional flow to steady-state and subsequent relaxation. The start-up period of the flow has been run to a total strain of 6. In (a) the results are shown for the FENE and FENE-PM models and in (b) results for the bead-rod chain and for a FENE dumbbell. The FENE dumbbell stress and birefringence in (b) have been rescaled by assuming that $b = 3N$. For the FENE and bead-rod chains, during the start-up the data follow the left branch of the loop and flow is stopped at the peak of the loop. Relaxation then proceeds down the right branch. For the FENE-PM model in (a) the start-up and relaxation fall on the same curve.

instantaneous end-to-end configuration. During the subsequent relaxation, we have already seen that the stress and birefringence of the FENE-PM, FENE and FENE-P all follow a single master curve for large values of Wi. This curve is a unique function of the instantaneous configuration of the chain and is given by the quasi-static nonlinear connector force law; i.e.

$$\frac{\tau_{11}^{p}-\tau_{22}^{p}}{b}=\left[\frac{1}{1-\Delta'/(N-1)}\right]\frac{\Delta'}{N-1} \tag{9}$$

We now turn to a discussion of the scaling of the FENE data. First we consider the relaxation portion of the curve. The steady-state value of the stress and birefringence both scale as b for large Wi. We have already shown that the initial stress decay-rate for the FENE is independent of b, cf. Eq. (7). Making the same assumptions as were used to derive Eq. (7), it can easily be shown that the initial decay of the steady-state birefringence for the FENE model is $\mathrm{d}\Delta'/\mathrm{d}(t/\lambda_H) = -b\mathrm{Wi}^{\mathrm{FENE}}$. Thus the initial rate of change of the scaled birefringence Δ'/b will be independent of b. Furthermore, the distribution of dumbbell lengths at steady-state is narrow and will remain narrow during the initial relaxation after flow is stopped because velocity of the dumbbell beads, and hence the trajectory, is dominated by the contribution from the spring force. What is most intriguing is the collapse of the data on the upper branch of the loop for various values of b during the onset of uniaxial elongation at each value of Wi. Since, at the inception of flow, the stress and birefringence are co-linear, the collapse of the data suggests a similarity in the stress and birefringence rates of change, but we are unable to derive any simple scalings for these without using preaveraging which will eliminate the hysteresis.

We also observe hysteresis in the stress versus birefringence for the bead-rod chain. In Fig. 13(b) we plot the scaled stress (divided by $N-1$) versus scaled birefringence (divided by $N-1$. For comparison, we also show the data for a FENE dumbbell with $b=150$ at $\mathrm{Wi}^{\mathrm{FENE}}=10.65$. In scaling the FENE dumbbell results in Fig. 13(b) we have again used the relationship $b=3N$ The bead-rod chain simulations qualitatively show the same trend in the hysteresis as found for the FENE model in Fig. 13(a). The bead-rod data collapse onto a single curve for $N=50, 100, 200$ at $\mathrm{Wi}=10.65$. The collapse of the data during relaxation follows directly from the universal stress and birefringence relaxation in Figs. 4 and 5. The extent of the hysteresis for bead-rod chains at $\mathrm{Wi}=10.65$ is qualitatively and quantitatively similar to that predicted for the FENE dumbbell. The hysteresis is smaller at $\mathrm{Wi}=3.55$ and the relaxation branch of the loop follows the relaxation from $\mathrm{Wi}=10.65$. The small difference initially in the $\mathrm{Wi}=3.55$ and $\mathrm{Wi}=10.65$ relaxation curves is due to the difference in the relaxation of the birefringence which will decrease with increasing N, cf. Fig. 5.

We now turn to a discussion of the numerical and physical origins of the stress-birefringence hysteresis. Hysteresis occurs in the FENE model because the distribution of dumbbell lengths during the start-up of extensional flow is very broad [27]. As time increases, dumbbells begin to accumulate near the maximum extension, but the distribution has a large shoulder which spans most dumbbell lengths [27]. This distribution is not well-approximated as a Gaussian [27]. The dumbbells near maximum extension become the dominant contributors to the stress due to the highly nonlinear restoring force whereas the birefringence has contributions that scale linearly with the length of each dumbbell. At steady-state the distribution is nearly a δ function and (during relaxation from steady state) is well approximated as a Gaussian. Thus for a given average birefringence, or dumbbell stretch, the stress can be larger during start-up than relaxation because of the aforementioned skewed distribution function.

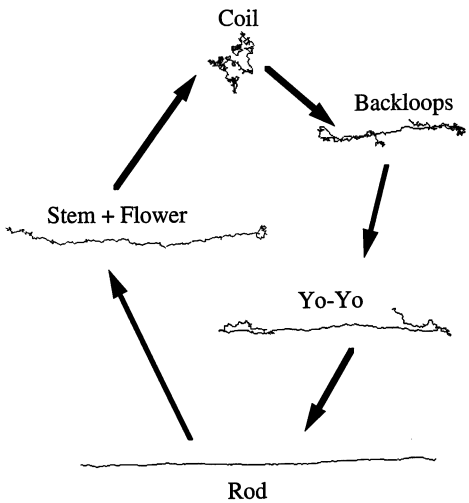

Fig. 14. Sample chain configurations for $N = 200$ during start-up of extensional flow at $\mathrm{Wi} = 10.65$ and relaxation. During start-up the chain goes from: Coil → Backloops → Yo-Yo → Rod. The relaxation proceeds as: Rod → Stem + Flower → Coil.

The previous argument also applies to the bead-rod chain, but there is another important aspect to the bead-rod chain hysteresis not present in the FENE dumbbell, namely configuration hysteresis. In Fig. 14 we show sample chain configurations for a chain during the start-up of extensional flow at $\mathrm{Wi} = 10.65$ with $N = 200$ and during the relaxation. During start-up the chain first forms a series of backloops [33], then as the backloops unfold the chain resembles the Yo-Yo model of Ryskin [34] with a taut, highly extended midsection bounded by backloops at the ends. Ultimately the chain is stretched almost completely straight like a rod. During relaxation the chain initially develops modulations along the entire backbone and further relaxation occurs from the ends inward-similar to the flower + stem model of Brochard-Wyart and Buguin [29]. Eventually (after many relaxation times) the chain returns to a coiled state. We have visually examined the start-up and relaxation of several chains and found similar trends in configurations. The typical configurations of the chain during the start-up of flow and the relaxation are very different. Furthermore, the average deformation of the chain in the Yo-Yo and the stem + flower configurations is similar, and so is the birefringence, but the stress is larger for the Yo-Yo configuration due to the low configurational entropy of the taut midsection of the chain.

5. Comparison to experimental data

Recently Spiegelberg and McKinley [1] and Orr and Sridhar [2] have measured extensional polymer stresses for both the start-up and subsequent relaxation after flow stops using the filament stretching rheometer. While we cannot simulate large enough bead-rod chains to compare directly to the start-up and relaxation, we can compare their results to the universal relaxation curve, Fig. 4, for the bead rod chains. Before we can compare the experiments to the

simulations we need to calculate values for N, $n_p kT$ and λ_1. We follow the same method as Doyle and Shaqfeh [7] and Spiegelberg and McKinley [1], namely we define

$$b = 3N = \frac{6M_w \sin^2[\tan^{-1}(\sqrt{2})]}{C_\infty M_0}, \tag{10}$$

$$n_p kT = \eta^p/(2.369\ldots\lambda_1), \tag{11}$$

where M_w is the polymer molecular weight, C_∞ is the characteristic number of monomer units in a Kuhn step, M_0 is the monomer molecular weight and $2\tan^{-1}(\sqrt{2}) = 109.5°$ is the tetrahedral bond angle. Eq. (11) is based on the assumption that the polymer has a Zimm spectrum [21]. In Ref. [7] Doyle and Shaqfeh calculated $n_p kT = 1.53$ Pa and $b = 8665$ for the polystyrene-based Boger fluid of Spiegelberg and McKinley [1] giving $N = 2888$. Furthermore Spiegelberg and McKinley [1] report a relaxation time of $\lambda_1 = 2.9$ s based on the polymer stress relaxation after shear flow. The fluid used by Orr and Sridhar [2] is a PIB-based Boger fluid, Fluid A with $M_w = 1.2 \times 10^6$ g mol^{-1}. Tirtaatmadja and Sridhar [35] fit the steady-state shear viscosity for the same Fluid A to a single mode Oldroyd-B model and obtained a characteristic polymer relaxation time $\lambda_1 = 1.1$ s, a polymer contribution to the viscosity, $\eta^p = 7.81$ Pa s and solvent viscosity, $\eta^s = 11.22$ Pa s (the previous time and viscosities are shifted values [2] for 21.5°C, the operating temperature of Ref. [2]). Substituting the polymer viscosity into Eq. (11) gives $n_p kT = 3.0$ Pa. For PIB $M_0 = 56$ g mol^{-1}, $C_\infty = 6.7$ which substituting into Eq. (10) gives $N = 4270$.

In Fig. 15 we have compared the experimental data for the polystyrene Boger fluid and the PIB Boger fluid to the universal stress relaxation curve for bead-rod chains. The time in the experimental data has been shifted, by an additive term, such that the first point lies on the bead-rod chain curve. The data of Orr and Sridhar falls slightly above the bead-rod chain curve and is in fairly good agreement. The data of Spiegelberg and McKinley fall below the bead-rod chain curve and are qualitatively similar to the bead-rod chain curve and the data of Orr and Sridhar, i.e. a fast initial stress decay followed by a slower decay. Both sets of experimental data are for finite strains and the data of Orr and Sridhar is for the largest strains. The universal bead-rod chain curve is strictly valid for relaxation from steady-state and thus we expect to see better agreement with the experimental data as the strain increases. What is interesting is that the data lie on the bead-rod curve in a region in which the rate of relaxation is highly nonlinear.

Furthermore, in Eq. (4) we showed that the steady state extensional stress difference scaled with $(N-1)n_p kT$ is equal to $5.87\mathrm{Wi} - 2$ for large Wi. For $\mathrm{Wi} = 3.3$ and $\mathrm{Wi} = 2.31$ the stress calculated from Eq. (4) is equal to $17.4(N-1)n_p kT$ and $11.6(N-1)n_p kT$, respectively. This is in good agreement with the PIB data in which the initial stress is equal to and $20.1(N-1)n_p kT$ and $11.2(N-1)n_p kT$ at $\mathrm{Wi} = 3.3$ and $\mathrm{Wi} = 2.31$, respectively. Eq. (4) predicts a larger initial stress at $\mathrm{Wi} = 2.84, 9.45, 10.8$ than observed for the polystyrene data at the corresponding Wi. We expect the experimental polystyrene stress to be smaller than that calculated from Eq. (4) because the data is for moderate strains and would be expected to increase at larger strains. We note that the magnitude of the polymer stresses in Fig. 15 is much smaller than the $O(N^3 n_p kT)$ value calculated for a completely straight bead-rod chain [5,4], but is 3 orders of magnitude larger than the stress associated with the polymer zero shear viscosity.

To compare to the full start-up and relaxation we must resort to simpler elastic dumbbell models. In Fig. 16(a) we compare the start-up of extensional flow and relaxation for the polystyrene-based Boger fluid [8] to the FENE-PM-Zimm model and a FENE dumbbell at $\mathrm{Wi} = 2.84$. The small dashed lines show the continuation of the elastic dumbbell models to steady-state. The stress in the models has been made dimensional with $n_p kT = 1.53$ Pa and the FENE parameter was chosen such that $b \times M = 3N$, where $M = 1$ for the FENE model and 10 for the FENE-PM-Zimm. Previously, Doyle and Shaqfeh [7] demonstrated that the FENE dumbbell will underestimate the stress at small strains because it is a single mode model while the multimode FENE-PM-Zimm is in very good agreement with the experimental data. At large strains both models underpredict the polymer stress. After the flow is stopped, at a strain of 4.47, the models relax almost as a single exponential while the experimental data decay much more rapidly. At long times the polystyrene data and the models are in better agreement. It is clear though that the models and the data have different relaxation rates at long times. This then implies that the polystyrene shear stress and extensional stress have differing relaxation rates at long times (this follows from the fact that we have made time dimensionless with the shear stress relaxation time). This disparity could be partly due to gravitational forces becoming important

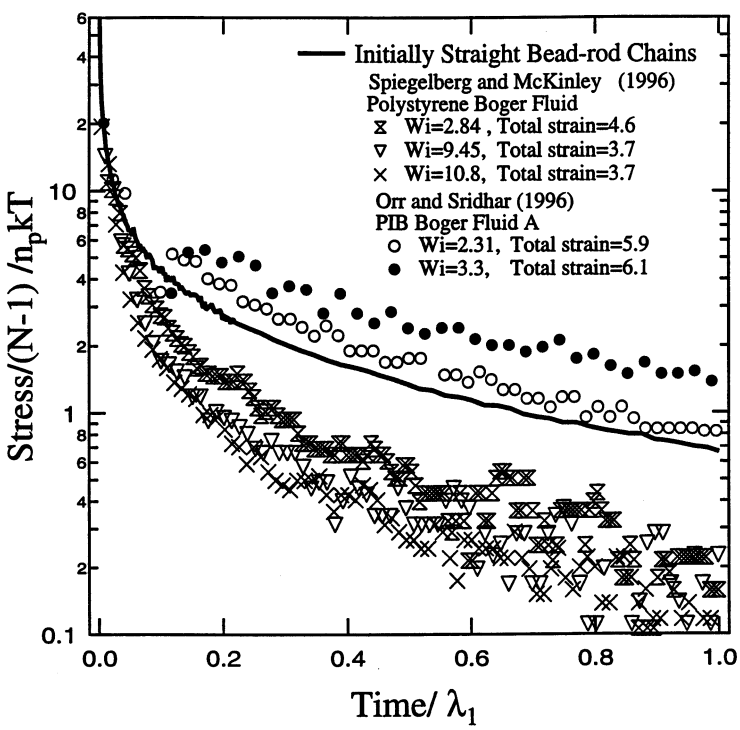

Fig. 15. Polymer stress made dimensionless with $n_p kT$ and divided by $(N-1)$ versus time scaled by the longest relaxation time. The solid line is the results for the initially straight bead-rod chains and the experimental results are the symbols. The time of the experiments has been shifted (by an additive term) such that the initial stress lies on the bead-rod chain universal curve. The experiments results are from Orr and Sridhar [2] and Spiegelberg and McKinley [1].

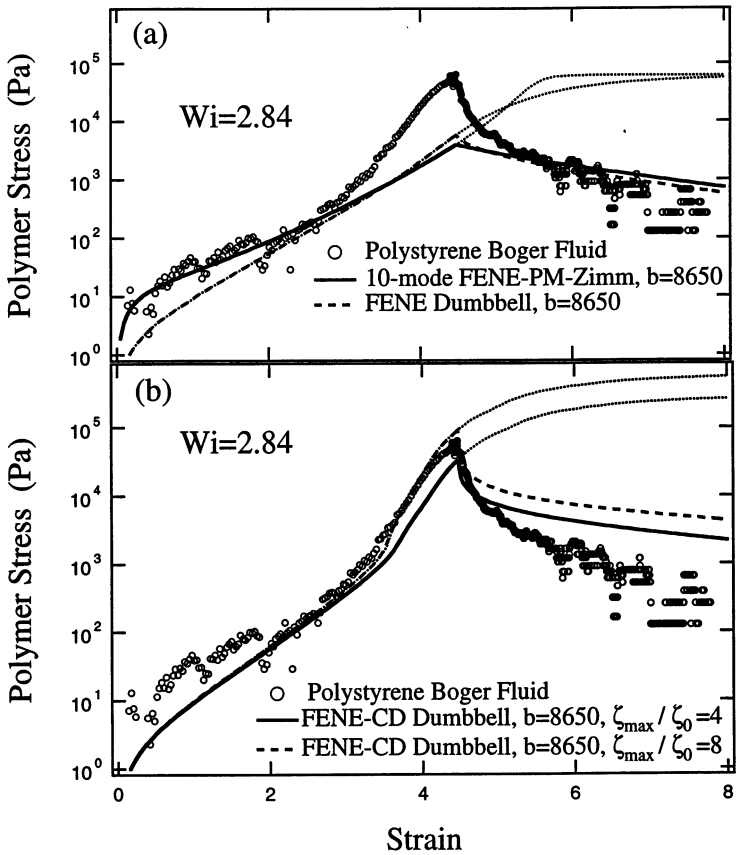

Fig. 16. Start-up and relaxation of the extensional polymer stress versus strain for a polystyrene Boger fluid from [8] and several dumbbell models at $\mathrm{Wi} = 2.84$. The thin dashed lines (for the dumbbell models) show the continuation of the stress to steady-state. The stress for the models has been made dimensional with $n_p kT = 1.54$ Pa.

and drainage effects in the filament stretching device rheometer at long times (strains of 7–8). Also shown in Fig. 16 are the results for the FENE and FENE-PM-Zimm models in which the flow has not been stopped. At large strains both models approach a stress which is comparable to the polystyrene stress at a strain of 4.47, before the flow is stopped.

In Fig. 16(b) we compare the same experimental polystyrene data to a conformation dependent FENE model, FENE-CD, with $\zeta_{max}/\zeta_0 = 4$ and 8. The FENE-CD with $\zeta_{max}/\zeta_0 = 8$ is in good agreement with the data for strains larger than 2 and up until the flow stops. When the flow stops, the FENE-CD models show a rapid decay in the stress, but this fast decay does not persist and gives rise to a much slower decay rate. The disparity in the polystyrene data and the elastic dumbbell models at strains of 5–7 cannot be attributed to drainage or gravitational effects.

In Fig. 17(a,b) we compare the birefringence divided by the stress-optic coefficient for the elastic models and experimental results for the polystyrene Boger fluid [8]. The birefringence of the polystyrene Boger fluid was also measured in the filament stretching rheometer, but the

experiment was operated in a plateau tank filled with a density matched fluid to reduce the effects of gravity as described in detail elsewhere [1]. The dimensionless stress-optic coefficient for all the dumbbell models is $C = 1/5$ [7,24]. Thus for the dumbbell models in Fig. 17 we have divided the dimensionless birefringence by 1/5 and multiplied by $n_p kT = 1.53$ Pa. For the polystyrene data we used a value $C = -5 \times 10^{-9}$ Pa^{-1} based on values reported in the literature for polystyrene in aromatic solvents [36–39]. The theoretical value of the stress-optic coefficient is [24,15]

$$C = \frac{2\pi}{45kT}\frac{(n^2+2)^2}{n}(\alpha_1 - \alpha_2).$$

For polystyrene, $n = 1.6$, $(\alpha_1 - \alpha_2) = -145 \times 10^{-25}$ cm^3 [40] giving $C = -6.4 \times 10^{-9}$ Pa^{-1}. For small strains all the models predict larger values for the birefringence than observed experimentally, but there is also significant scatter in the data at small strains ($\epsilon < 2$) related to the inherent resolution limit of the experiments. At larger strains the models slightly overpredict the birefringence. There is not a large difference in the FENE-CD and the FENE models during the start-up, cf. Fig. 17(a–b). In Fig. 17(a) the FENE-PM-Zimm and FENE birefringence relax very

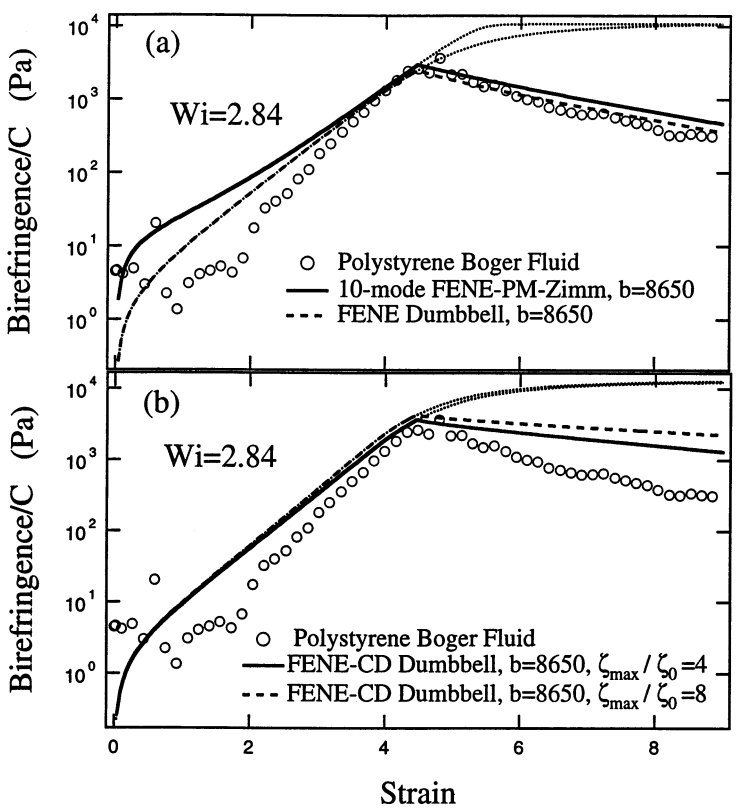

Fig. 17. Start-up and relaxation of the extensional birefringence divided by the stress optic coefficient versus strain for a polystyrene Boger fluid from [8] and several dumbbell models at Wi = 2.84. The thin dashed lines (for the dumbbell models) show the continuation of the birefringence to steady-state.

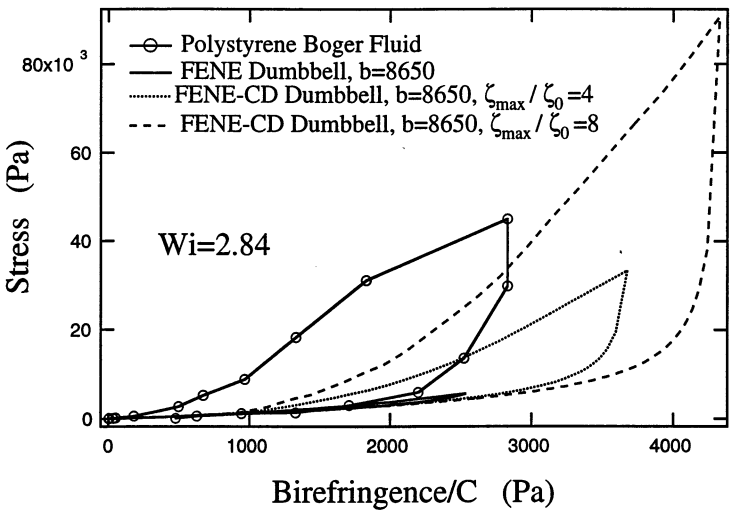

Fig. 18. Stress versus birefringence for the start-up of extensional flow and subsequent relaxation for a polystyrene based Boger fluid from [8] and the conformation dependent FENE model at Wi = 2.84. During start-up the data proceed along the left side of the hysteresis loop and during relaxation the data follows the right hand side of the loop.

similarly and are in good agreement with the birefringence data whereas the conformation dependent FENE birefringence in Fig. 17(b) releases significantly slower than the experimental data. The polystyrene birefringence relaxation can be well described by a single exponential decay with a characteristic time of approximately 3 s, in agreement with the shear stress decay rate. This is a better agreement than was found for the stress and is most probably due to the fact that the birefringence experiments were performed under conditions which minimize the effects of gravity.

In Fig. 18 we plot the stress versus birefringence for the polystyrene solution in Figs. 16 and 17 and the conformation dependent FENE. In Fig. 18 during start-up of flow the data follow the left hand side of the loops and relax down the right hand side. There is a hysteresis in the stress versus birefringence for the experimental data which is qualitatively captured by the dumbbell models and is similar to the hysteresis found for the bead-rod chains, cf. Fig. 13(b). We note that the largest hysteresis occurs when the stress and the birefringence are largest, corresponding to strains of 4–5 in Figs. 16 and 17 and thus within the regime in which errors due to gravity (stress) or baseline fluctuations due to small signals (birefringence) can be neglected. Thus the experiments confirm that there are multiple values for the stress at a given birefringence in extensional flows. Furthermore, the stress at a given value of the birefringence is larger during the start-up of flow than during the relaxation. We believe the physical reasons for this behavior are the same as found for the FENE and bead-rod chain models, namely the second moment of the distribution (or some similar scalar measure of the distribution) does not contain sufficient information to determine the polymeric stress and will underestimate the stress for strong flows. Additionally, in the more realistic bead-rod chain model, there is a configurational hysteresis in the conformation of the molecule that is not captured by a quasi-static estimate of the entropy associated with a specified end-to-end length.

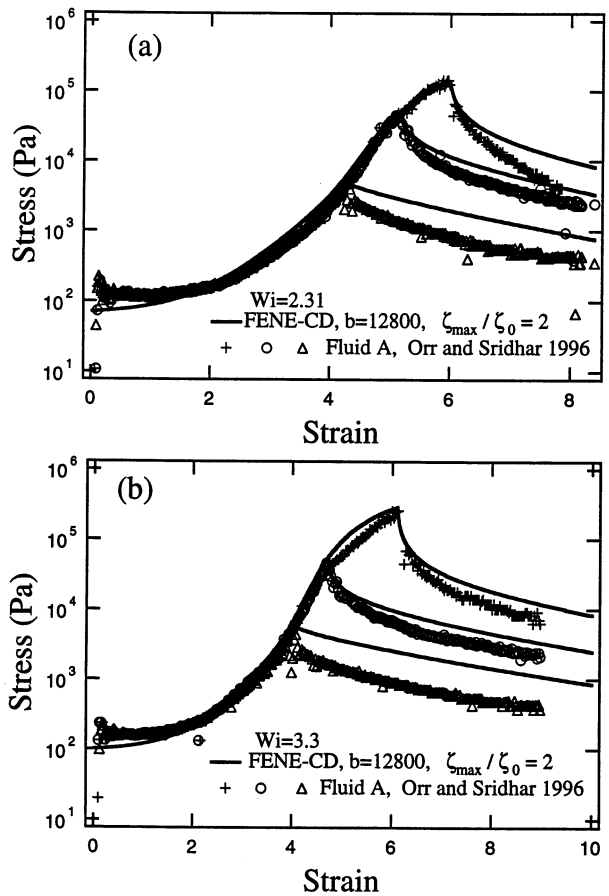

Fig. 19. Total extensional stress (polymer and solvent) versus strain during start-up and relaxation. The data of Orr and Sridhar [2] for Fluid A at (a) Wi = 2.31 ($\dot{\epsilon} = 2.1$ s) and (b) Wi = 3.3 ($\dot{\epsilon} = 3$ s) is compared to a conformation dependent FENE dumbbell with $b = 12\,800$ and $\zeta_{max}/\zeta_0 = 2$.

There are several factors which can contribute to the observed quantitative differences in the birefringence and stress for the experiments and elastic dumbbell models. First, in our comparison of the elastic dumbbell models to the bead-rod model we found that a multimode model describes the bead-rod chain data well at small strains while a single mode FENE model does well at large strains. Both the multimode FENE-PM and FENE models underpredict the relaxation rates of the bead-rod chains at intermediate strains. Secondly, we have incorporated the effects of hydrodynamic interactions into a FENE-CD model in a somewhat simplistic manner, though with physically reasonable parameters for the ratio of the maximum drag to the equilibrium (small deformation) drag, ζ_{max}/ζ_0. At intermediate degrees of chain stretch the relation between the chain stretch and the drag coefficient may not scale linearly with the chain stretch. Furthermore, the hysteresis in the chain configurations observed for the bead-rod chains during start-up and relaxation should also result in a hysteresis in the drag coefficient versus the average end-to-end distance of the chain.

Orr and Sridhar [2] have also measured extensional polymer solution stresses during the start-up and relaxation of extensional flow for PIB-based Boger fluids. The relaxation of the experimental stresses was already compared to the universal bead-rod chain relaxation curve in Fig. 15 and we compare the full start-up and relaxation to a FENE-CD in Fig. 19(a,b). Following the discussion earlier in this section, we set $n_p kT = 3$ Pa to make the FENE-CD stress dimensional and base the $\mathrm{Wi}^{\mathrm{FENE\text{-}CD}}$ on a relaxation time of $\lambda_1 = 1.1$ s. The solvent stress is taken to be 3 times the low Wi shear value, i.e. (11.22 Pa s [2]) multiplied by the extension rate. Since we do not know the initial aspect ratio of the sample we have not subtracted off the solvent stress in Fig. 19. A value of the drag ratio $\zeta_{\max}/\zeta_0 = 2$ in the FENE-CD model was found to give the best fit to the experimental data. This ratio is smaller than the upper bound calculated from Eq. (2), $\zeta_{\max}/\zeta_0 = 7.9$ (using $L = (b/3) \times 1.54$ nm, $L/R = \sqrt{b/3}$, $d = 0.5$ nm). The FENE-CD is in very good agreement with the experimental data beyond a strain $\epsilon \geq 1$ during start-up of the flow. At smaller strains ($\epsilon \leq 1$) the flow in the filament stretching rheometer is not purely uniaxial extension [41]. Additionally, the FENE-CD is a single mode model and thus will underpredict the polymer stress at small strains. After the flow is stopped, the FENE-CD model stress relaxes slower than the PIB data, but the difference between the simulation and the experimental data is not as large as was found for the polystyrene data in Fig. 16. The FENE-CD is in best agreement with the PIB data at the larger Wi, $\mathrm{Wi} = 3.3$, and at large strains. Overall the agreement between the simulations and the experimental data is quite good considering we have only varied one parameter, $\zeta_{\max}/\zeta_0$, and even this variation was bound by the value given by Eq. (2). All the other parameters in the elastic models have been chosen based on the molecular architecture of the polymer and the reported rheological properties.

6. Summary

We have investigated the relaxation of polymer chains following extensional flow. A universal relaxation curve for the stress decay from steady-state was found by shifting the results to lie on the curve described by the relaxation of an initially straight chain. For relaxation from steady-state the bead-rod chain, FENE dumbbell, FENE-P dumbbell and FENE-PM model demonstrate that the initial stress decays with an $\mathrm{O}(\mathrm{Wi}^2)$ rate. The universal stress relaxation curve compares favorably to experimental data for relaxation of polystyrene [1] and polyisobutylene Boger fluids [2] following extensional flow.

We have also shown that there is not a simple one-to-one relation in the stress and birefringence for the bead-rod model in extensional flow. Thus there is hysteresis in comparing the stress versus birefringence during the start-up of flow and subsequent relaxation. We have also shown that the FENE model shows very similar hysteresis while the FENE-PM model does not due to the preaveraging of the nonlinear terms. The bead-rod model also displays a configuration hysteresis which contributes to the stress-birefringence hysteresis. The hysteresis in the models is in qualitative agreement with recent experimental data [8]. These findings demonstrate the importance of pursuing numerical techniques such as CONNFFESSIT [42–44] and Brownian configuration fields [44,45] which do not preaverage nonlinear terms in constitutive equations.

Acknowledgements

The authors are grateful to Nick Orr and Tam Sridhar for providing the numerical values for their PIB data. This material is based upon work supported by the National Science Foundation under Grant No. DMR-9400354 and support for PSD through a Lieberman Fellowship.

Appendix A

In the test we have presented numerical simulations and scaling arguments which support the existence of a stress relaxation master curve following cessation of a homogeneous uniaxial elongational flow. Similar master curve characteristics are exhibited by bead-rod and bead-spring models, e.g. the FENE-PM chain and the FENE dumbbell (without the Peterlin approximation). It has been noted elsewhere [46] that the FENE-P dumbbell model also predicts a master curve that can be computed analytically. In this appendix we show how the general form for a number of the numerical results presented in this paper can also be obtained analytically from the FENE-P dumbbell constitutive equations.The evolution equation for the FENE-P dumbbell model in dimensionless form is

$$\mathrm{A}_{(1)} = -[f(tr\,\mathrm{A})\mathrm{A} - \mathrm{I}] \tag{12}$$

where the subscript (1) indicates the upper-convected derivative and time has been nondimensionalized with the characteristic relaxation time λ_H. The Weissenberg number is $\lambda_H\dot{\epsilon}$. We nondimensionalize in a manner consistent with the discussion in Section 2.2 in the text, and thus the second moment of the dumbbell configuration $\mathrm{A} = \langle \mathrm{QQ} \rangle$ is made dimensionless with $(N-1)a^2/3$ and $f(tr\,\mathrm{A}) = [1 - tr(\mathrm{A})/b]^{-1}$. Moreover, the dimensionless extensibility parameter is related to the number of Kuhn steps in a bead rod chain via the expression, $b = 3(N-1) \approx 3N$.The polymeric contribution to the stress is given by either the Kramers or Giesekus relationships

$$\tau^{\mathrm{p}} = f(tr\,\mathrm{A})\mathrm{A} - \mathrm{I} = \mathrm{A}_{(1)} \tag{13}$$

where stress is made dimensionless with $n_{\mathrm{p}}kT$.

In transient uniaxial elongation, Eq. (12) can be written as two coupled nonlinear ordinary differential equations

$$\frac{\mathrm{d}A^+}{\mathrm{d}\hat{t}} = 2\mathrm{Wi}A^- - fA^+ + 3, \tag{14}$$

$$\frac{\mathrm{d}A^-}{\mathrm{d}\hat{t}} = \mathrm{Wi}(A^+ + 3) - fA^-, \tag{15}$$

where $A^+ = A_{11} + 2A_{22}$, $A^- = A_{11} - A_{22}$, $\hat{t} = t/\lambda_H$, and $f = b/(b - A^+)$. Note in this context that 1 refers the coordinate along the principle axis of extension of the uniaxial elongational flow and *2* is any coordinate perpendicular to the 1 direction.

Asymptotic steady-state values for $\mathrm{Wi} > 1/2$ and $b \gg 1$ of the FENE connector and the stress difference are given by $f \to 2\mathrm{Wi}$ and $A^- \to b[(1 - 3/b) - 1/(2\mathrm{Wi})]$. The steady-state stress difference then becomes

$$\tau_{11}^{p} - \tau_{22}^{p} = \Delta\tau^{p} = (2\mathrm{Wi})b[(1 - 3/b) - 1/(2\mathrm{Wi})]. \tag{16}$$

Since the longest relaxation time scales as $\lambda \approx \mathrm{N}^2$ for a Rouse (or bead-rod) chain, the initial stress therefore varies as $\Delta\tau^{p} \approx N^3$ as is also found for bead-rod chains.

Following cessation of uniaxial elongation from a steady state configuration at large final Hencky strains $\epsilon_f = \dot{\epsilon} t_f \gg 1$, Eqs. (14) and (15) can be simplified by setting $\mathrm{Wi} = 0$, and are then decoupled from each other. Implicit transcendental expressions for $A^{+}(t)$ and $A^{-}(t)$ can be obtained by direct integration, and simpler explicit expressions can also be obtained for short times and long times following cessation of elongation. For short times $(t - t_f)/\lambda_H \ll 1$, the dimensionless stress difference can be expressed in the form

$$\frac{\tau_{11}^{p} - \tau_{22}^{p}}{b} = \frac{[(1 - 3/b)(2\mathrm{Wi})^{-1} \exp[(2\mathrm{Wi})^{-1}]] \exp(-\sqrt{2\Gamma})}{\sqrt{2\Gamma}}, \tag{17}$$

where the dimensionless 'reduced time' Γ is given by

$$\Gamma = \frac{t - t_f}{\lambda_H} + a_{\mathrm{Wi}} = \frac{t - t_f}{\lambda_H} + \frac{1}{8(\mathrm{Wi})^2} \tag{18}$$

The polymeric stress (scaled with $n_p kTb = 3n_p kT(N - 1)$) therefore follows a single relaxation master curve if the physical elapsed time $t - t_f$ is shifted by an additive shift factor a_{Wi} given by Eq. (18). This additive shift factor therefore scales as $(\mathrm{Wi})^{-2}$ as also found for bead-rod chains and FENE dumbbells.

The dimensionless birefringence Δ' predicted by a FENE-P dumbbell model is simply given by the expression, $\Delta = A^{-}(t)$. This follows since the configuration probability distribution function remains Gaussian at all times [47]. The scaled birefringence at short times $(t - t_f)/\lambda_H \ll 1$ is therefore given by

$$\frac{\Delta}{(N - 1)} = 3[1 - 3/b - (\mathrm{Wi}) - 1] \exp[(2\mathrm{Wi}) - 1] \exp(-\sqrt{2\Gamma}), \tag{19}$$

And relaxes more slowly than the polymeric stress in agreement with the calculations presented in Fig. 3.At long times $(t - t_f)/\lambda_H \gg 1$ the stress becomes

$$\frac{\tau_{11}^{p} - \tau_{22}^{p}}{b} = (1 - f_{eq}/(2\mathrm{Wi})) \exp[1 - f_{eq}/(2\mathrm{Wi})] \exp[-(t - t_f)/\lambda_H], \tag{20}$$

where $f_{eq} = (1 + 3/b)$ is the equilibrium value of the FENE connector. At long times, the polymeric stress therefore follows a simple decaying exponential in time that is a factor of $(2\mathrm{Wi}) \exp[1 - (2\mathrm{Wi})^{-1}]$ lower than that predicted by stress relaxation for the linear Oldroyd-B model.

In order to extend a FENE-P dumbbell to full extension, an infinite Weissenberg number is required; however, for all finite Wi, the initial value of the stress and its evolution at short times follows a power-law similar to those shown in Fig. 5. At large Wi and for very short times, the exponential terms in Eq. (17) can be neglected and the stress difference then relaxes as

$$\frac{\tau_{11}^{p} - \tau_{22}^{p}}{N - 1} = \frac{3}{\sqrt{2}} \Gamma^{-1/2}, \tag{21}$$

from an initial value given by Eq. (16) at an initial reduced time of $1/[8(\mathrm{Wi})^2]$. The numerical value $3/\sqrt{2} \approx 2.12$ in Eq. (21) is comparable to the value of 1.67 found from the bead-rod calculations and the value of 1.49 reported by Grassis and Hinch.Finally, Eq. (17) can be used to obtain an estimate for the time-scale denoted $\lambda_{50\%}$ at which the stress has fallen to 50% of the initial plateau value. Using the result from Eq. (16) as the initial plateau value and upon substituting half this value into Eq. (17), we find that, for $\mathrm{Wi} > 0.5$,

$$\frac{\lambda_{50\%}}{\lambda_H} = \frac{1}{2}(1 + \mathrm{Wi}\exp(-1/2\mathrm{Wi}))^{-2} - \frac{1}{8\mathrm{Wi}^2} \tag{22}$$

which for $\mathrm{Wi} \gg 1$ can be simplified to

$$\frac{\lambda_{50\%}}{\lambda_H} = \frac{3}{8\mathrm{Wi}^2} \tag{23}$$

This prediction for $\lambda_{50\%}$ is shown in Fig. 6 by the dashed line.

References

[1] S.H. Spiegelberg and G.H. McKinley, Stress relaxation and elastic decohesion of viscoelastic polymer solutions in extensional flow, J. Non-Newtonian Fluid Mech. 67 (1996) 49–76.
[2] N.V. Orr and T. Sridhar, Stress relaxation in uniaxial extension, J. Non-Newtonian Fluid Mech. 67 (1996) 77–103.
[3] J. van Niewlcoop and M.M.O. Muller von Czerniclci, Elongation and subsequent relaxation measurements on dilute polyisobutylene solutions, J. Non-Newtonian Fluid Mech. 67 (1996) 105–123.
[4] P.S. Grassia and E.J. Hinch, Computer simulations of polymer chain relaxation via Brownian motion, J. Fluid Mechanics, 208 (1996) 255–288.
[5] P.S. Doyle, E.S.G. Shaqfeh, and A.P. Gast, Dynamic simulation of freely draining, flexible polymers in linear flows, J. Fluid Mech. 334 (1997) 251–291.
[6] J.M Rallison, Dissipative stresses in dilute polymer solutions, J. Non-Newtonian Fluid Mech. 68 (1997) 61–83.
[7] P.S. Doyle and E.S.G. Shaqfeh, Dynamic simulation of freely-draining, flexible bead-rod chains: Start-up of extensional and shear flow, Submitted to J. Non-Newtonian Fluid Mech. (1997).
[8] S.H. Spiegelberg and G.H. McKinley, Elastic and viscous contributions to stress in extensional rheometry of viscous polymer solutions, in: XIth International Congress on Rheology, Quebec City, pp. 211–212, 1996.
[9] H.A. Kramers, The viscosity of macromolecules in a streaming fluid, Physica 11 (1944) 1–19.
[10] R.B. Bird, C.F. Curtiss, R.C. Armstrong, and O. Hassager, Dynamics of Polymeric Liquids: Volume 2 Kinetic Theory, Wiley, New York, 1987.
[11] W.B. Russel, D.A. Saville, and W.R Schowalter, Colloidal Dispersions, Cambridge University Press, Cambridge, 1989.
[12] H.C. Ottinger, Stochastic Processes in Polymeric Fluid. Springer, Berlin, 1995.
[13] T.W. Liu. Flexible polymer chain dynamics and rheological properties in steady flows, J. Chem. Phys. 90 (1989) 5826–5842.
[14] G.G. Fuller, Optical Rheometry of Complex Fluids, Oxford University Press, London, 1995.
[15] W. Kuhn and F. Grun, Relationships between elastic constants and stretching double refraction of highly elastic substances, Kolloid Z. 101 (1942) 248.
[16] H.R. Warner, Kinetic theory and rheology of dilute suspensions of finitely extendible dumbbells, Ind. Eng. Chem. Fundam. 11 (1972) 379–387.
[17] M. Herrchen and H.C. Ottinger, A detailed comparison of various FENE dumbbell models, J. Non-Newtonian Fluid Mech. 68 (1997) 17–42.

[18] P.G. de Gennes, Coil-stretch transition in dilute flexible polymers under ultrahigh velocity gradients, J. Chem. Phys. 60 (1974) 5030–5042.
[19] E.J. Hinch, Proc. Symp. Polym. Lubrification, Brest, France, 1974.
[20] G.G. Fuller and L.G. Leal, Flow birefringence of dilute polymer solutions in two dimensional flows, Rheol. Acta 19 (1980) 580–600.
[21] M. Doi and S.F. Edwards, The Theory of Polymer Dynamics, Oxford Science Publications, Oxford, 1986.
[22] R.G. Larson, The Structure and rheology of complex fluids, in press, 1997.
[23] L.E. Wedgewood, D.N. Ostrov, and R.B. Bird, A finitely extensible bead-spring chain model for dilute polymer solutions, J. Non-Newtonian Fluid Mech. 40 (1991) 199–139.
[24] R.G. Larson, Constitutive Equations for Polymer Melts and Solutions, Butterworth, Guildford, UK, 1988.
[25] J.H. Ferziger, Numerical Methods for Engineering Application, Wiley, New York, 1981.
[26] O. Hassager, Kinetic theory and rheology of bead-rod models for macromolecular solutions. I. Equilibrium and steady flow, J. Chem. Phys. 60 (1974) 2111–2124.
[27] R. Keunings, On the Peterlin appoximation for finitely extensible dumbbells, J. Non-Newtonian Fluid Mech. 68 (1997) 85–100.
[28] T.T. Perkins, S.R. Quake, D.E. Smith, and S. Chu, Relaxation of a single DNA molecule observed by optical microscopy, Science 264 (1994) 822–825.
[29] F. Brochard-Wyart and A. Buguin, Polymer chains under strong flow: Stems and flowers, MRS Bull. 22 (1997) 48–52.
[30] S.F. Smyth, Chen-Hua Liang, M.E. Mackay, and G.G. Euller, The stress jump of a semirigid macromolecule after shear: comparison of the elastic stress to the birefringence, J. Rheology 40 (1995) 659–672.
[31] M.D. Chilcott and J.M. Rallison, Creeping flow of dilute polymer solutions past cylinders and spheres, J. Non-Newtonian Fluid Mech. 29 (1988) 381–432.
[32] J. Azaiez, R. Guenette, and A. Ait-Kadi, Numerical simulation of viscoelastic flows through a planar contraction, J. Non-Newtonian Fluid Mech. 62 (1996) 253–277.
[33] J.M. Rallison and E.J. Hinch, Do we understand the physics in the constitutive equation? J. Non-Newtonian Fluid Mech. 29 (1988) 37–55.
[34] G. Ryskin, Calculation of the effect of polymer additive in a converging flow, J. Fluid Mech. 178 (1987) 423–440.
[35] V. Tirtsatmadja and T. Sridhar, Comparison of constitutive equations for polymer solutions in uniaxial extension, J. Rheol. 39 (1995) 1133–60.
[36] P. Munk and A. Peterlin, Streaming birefringence, Rheol. Acta 9 (1970) 288–293.
[37] A.S. Lodge, A network theory of flow birefringence and stress in concentrated polymer solutions, Trans. Farad. Soc. 52 (1956) 120–130.
[38] J.L.S. Wales and H. Janeschitz-Kriegel, Effects of concentration and polydispersity on flow birefringence of polystyrene, Rheol. Acta 7 (1968) 19–23.
[39] W. Philippoff, in: Proc. IV Intern. Congr. Rheol., Interscience Publications, 1963.
[40] J. Brandrup and E.H. Immergut, Polymer Handbook, Wiley, New York, 1989.
[41] S.H. Spiegelberg, G.H. Ables, D.C. McKinley, The role of end-effects on measurements of extensional viscosity in filament stretching rheometers, J. Non-Newtonian Fluid Mech. 64 (1996) 229–267.
[42] M. Laso, H.C. Ottinger, Calculation of viscoelastic flow using molecular models: the CONNFFESSIT approach, J. Non-Newtonian Fluid Mech. 47 (1993) 1–20.
[43] K. Feigl, M. Laso, and H.C. Ottinger, CONNFFESSIT Approach for solving a two-dimensional viscoelastic fluid problem, Macromolecules 28 (1995) 3261–3274.
[44] H.C. Ottinger, B.H.A.A. van den Brule, M.A. Hulsen, Brownian configurational fields and variance reduced CONNFFESSIT, preprint, 1997.
[45] M.A. Hulsen, A.P.G. van Heel, B.H.A.A. van den Brule, Simulation of viscoelastic flows using Brownian configuration fields, J. Non-Newtonian Fluid Mech., in press, 1996.
[46] G.H. McKinley, Extensional Rheology and Flow Instabilities in Elastic Polymer Solutions Dynamics of Complex Fluids, in: M.J. Adams (ed.), Proceedings of the Royal Society, Unilever Indo, UK Forums, Vol. 1, J. Imperial College Press, London, 1997.
[47] R. Keunings, On the peterlin approximation for finitely extensible dumbbells, J. Non-Newtonian Fluid Mech. 68 (1997) 85–100.